DMD Fast Forward. Published on December 7, 2022 as DOI: 10.1124/dmd.122.001024
This article has not been copyedited and formatted. The final version may differ from this version.

# Contribution of UGT enzymes to human drug metabolism stereoselectivity: a case study of medetomidine, RO5263397, propranolol and testosterone

Nicolò Milani, NaHong Qiu and Stephen Fowler

Pharmaceutical Sciences, Roche Pharma Research and Early Development, Roche Innovation Centre Basel, Grenzacherstrasse 124, 4070, Basel, Switzerland (NM, NQ, SF) and Department of Chemistry, Biology and Biotechnology, University of Perugia, 06123 Perugia, Italy (NM).

DMD Fast Forward. Published on December 7, 2022 as DOI: 10.1124/dmd.122.001024
This article has not been copyedited and formatted. The final version may differ from this version.

**Running title:** Impact of UGT Stereoselectivity on Drug Clearance

**Corresponding Author**: Stephen Fowler, Ph.D.

Pharmaceutical Sciences, Roche Pharmaceutical Research and Early Development, Grenzacherstrasse 124, CH-4070 Basel, Switzerland.

Tel.: +41-61-68-85105

E-mail: stephen.fowler@roche.com

Text pages: 29

Tables: 4

Figures: 5

References: 34

Abstract: 219 (250)

Significance Statement: 74 (80)

Introduction: 663 (750)

Discussion: 1488 (1,500)

## Abbreviations

UGT, uridine diphosphate glucuronosyl transferase; UDPGA, uridine diphosphate glucuronic acid; CYP, cytochrome P450; NADPH, reduced nicotinamide adenine dinucleotide phosphate IVIVE, in Vitro–In Vivo Extrapolation BSA, bovine serum albumin; DDI, drug-drug interaction; HLM, human liver microsomes; CLM, cynomolgus monkey liver microsomes; RLM, rat liver microsomes; MPLM, pooled Gottingen minipig liver microsomes; DLM, dog liver microsomes; MLM, mouse liver microsomes; HKM, human kidney microsomes; HIM, human intestinal microsomes LC-MS/MS, liquid chromatography coupled with tandem mass spectrometry; UHPLC, ultra-High-Performance Liquid Chromatography DMSO, dimethyl sulfoxide ; $CL_{int}$, intrinsic clearance; $CL_{p,}$ plasma bound clearance; BW, body weight; MPPGL, microsomal protein per gram of liver; AGP, alpha(1)-acid glycoprotein; BQL, below limit of quantification; BPP, Blood to plasma partitioning.

DMD Fast Forward. Published on December 7, 2022 as DOI: 10.1124/dmd.122.001024
This article has not been copyedited and formatted. The final version may differ from this version.

**Abstract**

The enantiomeric forms of chiral compounds have identical physical properties but may vary greatly in their metabolism by individual enzymes. Enantioselectivity in UDP-glucuronosyl transferase (UGT) metabolism has been reported for a number of compounds and with different UGT isoforms involved. However, the impact of such individual enzyme results on overall clearance stereoselectivity is often not clear. The enantiomers of medetomidine, RO5263397, and propranolol and the epimers testosterone and epitestosterone exhibit more than 10-fold difference in glucuronidation rates by individual UGT enzymes. In this study we examined the translation of human UGT stereoselectivity to hepatic drug clearance considering the combination of multiple UGTs to overall glucuronidation, the contribution of other metabolic enzymes such as cytochromes P450, and the potential for differences in protein binding and blood/plasma partitioning. For medetomidine and RO5263397, the high individual enzyme (UGT2B10) enantioselectivity translated into ~3- to >10-fold differences in predicted human hepatic in vivo clearance. For propranolol the UGT enantioselectivity was irrelevant in the context of high cytochrome P450 (CYP) metabolism. For testosterone a complex picture emerged, due to differential epimeric selectivity of various contributing enzymes and potential for extrahepatic metabolism. Quite different patterns of CYP and UGT-mediated metabolism were observed across species, as well as differences in stereoselectivity, indicating that extrapolation from human enzyme and tissue data is essential when predicting human clearance enantioselectivity.

DMD Fast Forward. Published on December 7, 2022 as DOI: 10.1124/dmd.122.001024
This article has not been copyedited and formatted. The final version may differ from this version.

**Significance Statement**

Individual enzyme stereoselectivity illustrates the importance of three dimensional drug-metabolizing enzyme-substrate interactions and is essential when considering the clearance of racemic drugs. However, translation from in vitro to in vivo can be challenging as contributions from multiple enzymes and enzyme classes must be combined with protein binding and blood/plasma partitioning data to estimate the net intrinsic clearance for each enantiomer. Preclinical species may be misleading as enzyme involvement and metabolism stereoselectivity can differ substantially.

DMD Fast Forward. Published on December 7, 2022 as DOI: 10.1124/dmd.122.001024
This article has not been copyedited and formatted. The final version may differ from this version.

## Introduction

Chiral compounds contain one or more structural elements which can take up only one of two non-superimposable mirror image forms. This is most frequently due to a carbon atom having bonds to four different chemical substituents in a tetrahedral arrangement. Pairs of mirror image molecules (enantiomers) have the same physicochemical characteristics (such as molecular weight, lipophilicity, solubility and permeability). In chiral environments such as enzymatic active sites, the enantiomers may have different binding interactions and consequently different metabolism rates and inhibition potency. These characteristics make pairs of enantiomers interesting for enzyme structure-function studies since altered activity must originate from the stereochemistry difference. Another form of stereoisomerism is represented by epimers, which contain multiple chiral centers but differ from each other for the configuration of one center and may have differences in physicochemical properties.

Chiral drugs may be administered as racemic mixtures (mix of both enantiomers) or enantiopure drugs (single enantiomeric form). The use of pure enantiomer drugs has increased in recent years due to the advance of stereoselective synthetic methodologies and purification processes. However, especially for older drug compounds, a racemic mixture of enantiomers may have been developed if the safety profile of the mixture was acceptable. Single enantiomer small molecule drugs comprised 55% of the total FDA approved drugs in the period 2001-2010 (Agranat et al., 2012). In contrast, achiral and racemic drugs accounted for 32% and 13%, respectively. Advantages of developing a pure enantiomer drug include: 1) improved therapeutic index; 2) reduced perpetrator DDI potential; 3) lower total dosage (Agranat et al., 2012; Calcaterra and D'Acquarica, 2018). Although the production of racemates may simplify chemical processing (enantioselective synthesis and purification not needed), the biological characterization for both enantiomers is still required for new drugs (Calcaterra and D'Acquarica, 2018).

DMD Fast Forward. Published on December 7, 2022 as DOI: 10.1124/dmd.122.001024
This article has not been copyedited and formatted. The final version may differ from this version.

RO5263397 is a single enantiomer drug candidate formerly under development for the treatment of schizophenia. In vivo and in vitro studies showed that the pure enantiomer RO5263397 was cleared via UGT2B10 glucuronidation with a minor contribution from UGT1A4 (Fowler et al., 2015). In subsequent experiments RO5263397 was found to be the most selective of known UGT2B10 metabolized drugs when considering a combination of CYP and UGT-mediated metabolism processes (Milani et al., 2020). The observation of significant stereoselectivity differences in the intrinsic clearance of RO5263397 and its enantiomer RO5263396 raised the question of whether these in vitro effects would have in vivo relevance. A search for drugs with reports of stereoselective UGT-mediated metabolism identified 8 candidates: oxazepam, flurbiprofen, medetomidine, etodolac, carvedilol, naproxen and testosterone. Medetomidine, propranolol and testosterone were commercially available as enantiomerically pure substances and had literature reports of substantial UGT enantioselectivity (Table 1). Note: testosterone and epitestosterone differ in stereochemistry of one out of several chiral centers and are therefore epimers, which may differ in physicochemical properties.

A number of processes can contribute to differential drug clearance of chiral compounds. For most drugs, UGT enzymes are not the sole contributors to metabolism, with cytochrome P450 and other enzymes also involved. In addition, stereoselective protein binding may occur (e.g. as reported for flurbiprofen (Davies, 1995), etodolac, indoprofen, ibuprofen, and ketoprofen (Coelho et al., 2021)) which may impact both metabolism and renal filtration clearance processes. In this work we have investigated the metabolism of 4 pairs of compounds where significant metabolism stereoselectivity differences were exhibited by individual UGT isoforms (see Figure 1A for chemical structures). We have taken a stepwise approach for assessing the likely in vivo relevance of individual UGT enzyme stereoselectivity, as illustrated in Figure 1B: (1) Initial observation that a drug is stereoselectively metabolized by a given UGT. (2) Result confirmation using systems (e.g. microsomes) containing multiple UGT enzymes. (3) Additional experiments to assess the

contribution of non-UGT enzymes. (4) Prediction of hepatic clearance taking into account protein binding and blood/plasma partitioning. Potential future steps to include IVIVE for extrahepatic metabolism and non-metabolic clearance are also indicated in this diagram. Comparison of UGT stereoselectivity using liver microsomes from 5 animal species was also performed to assess species differences in metabolism stereoselectivity.

DMD Fast Forward. Published on December 7, 2022 as DOI: 10.1124/dmd.122.001024
This article has not been copyedited and formatted. The final version may differ from this version.

## Materials and Methods

### Materials

RO5263397, RO5263396, and (+)-(S)-medetomidine (dexmedetomidine) were synthesized at Roche (Basel, Switzerland). Alamethicin and UDPGA were purchased from Sigma-Aldrich (St. Louis, MO, USA). (-)-(R)-medetomidine (levomedetomidine), (-)-(R)-propranolol, (+)-(S)-propranolol, testosterone and epitestosterone and purchased from Toronto Research Chemicals (North York, Ontario, Canada). 150-donor mixed gender pooled human liver microsomes (HLM), pooled male cynomolgus liver microsomes (CLM), pooled male Wistar Han rat liver microsomes (RLM), pooled male Gottingen minipig (MPLM-m), pooled male CD-1 mouse microsomes (MLM), and recombinant expressed UGTs 1A4 and 2B10 were purchased from Corning (Corning, New York, USA). 8-donor mixed gender pooled human kidney microsomes (HKM) and 15-donor mixed gender pooled human intestinal microsomes (HLMs) were purchased from Xenotech (Kansas City, USA). Pooled male beagle dog microsomes (DLM) was purchased from BD Biosciences (Woburn, MA, US). Tris buffer was purchased from Invitrogen (Carlsbad, CA, USA). A highly flexible automated in vitro metabolism system (Badee et al., 2018) was implemented on a Tecan Fluent system (Tecan Group Ltd, Männedorf, Switzerland) and used to perform these studies at Hoffmann-La Roche Ltd (Basel, Switzerland).

### Methods

**Glucuronidation metabolism timecourse experiments for intrinsic clearance determination in presence and absence of BSA**. RO5263397, RO5263396, testosterone, epitestosterone, and both enantiomers of medetomidine and propranolol were dissolved in DMSO as stock solutions. Pooled HLM, HIM, and HKM were prepared in Tris-HCl buffer (100 mM, pH 7.5) containing 10 mM magnesium chloride ($MgCl_2$) at a microsomal protein concentration of 1.1 mg/mL (final reaction concentration: 1 mg/mL) and then were pre-treated with alamethicin (10 µg/ mg protein) for 30 min

DMD Fast Forward. Published on December 7, 2022 as DOI: 10.1124/dmd.122.001024
This article has not been copyedited and formatted. The final version may differ from this version.

on ice. Parallel incubations with HLM, HIM, and HKM were performed in the presence of BSA (2% w/v) which was added to the Tris-HCl buffer before alamethicin conditioning. Prepared microsomes were combined with UDPGA (5 mM final concentration) and warmed to 37 °C over 5 minutes in 96-well deep-well plates. Reactions (400 µL final volume) were initiated by addition of 1 µL test drug in DMSO (0.25% v/v final DMSO concentration) and mixing. After incubation times of 0.5, 3.5, 6.5, 10, 15, 20, 30, and 45 minutes 40 µL of each incubation mixture was removed and pipetted into 384-well deep well plates preloaded with 80 µL quench solution (chilled acetonitrile containing 500 ng/mL of $D_6$-midazolam as internal standard). Quenched samples from all incubations were chilled on ice for 30 minutes before centrifugation (20,000x g, 10 minutes). The supernatant of each sample was removed and analyzed by LC-MS/MS. All the experiments described above were performed as replicates of four.

**CYP metabolism timecourse experiments for intrinsic clearance determination.** Human microsomes were prepared in potassium phosphate pH 7.4 (100 mM, pH 7.4) at a microsomal protein concentration of 1.1 mg/mL (final reaction HLM concentration: 1 mg/mL). CYP metabolism experiments were performed using well-established CYP incubation conditions (Walsky and Obach, 2004) rather than in a combined UGT/CYP incubation. This was because CYP turnover was lower for some substrates if tested under the conditions used for UGT incubations. Incubations were made by spiking test compounds (final solvent content of 0.25% v/v DMSO) into prepared HLM solutions and warming to 37 °C over 5 minutes in 96-well deep well plates. Reactions were started by the addition of 40 µl 10 x concentrated NADPH stock solution prewarmed to 37 ºC. Final NADPH concentration was 1 mM, and total reaction volume was 400 µL. The method followed the same sampling times and sample preparation as for the glucuronidation metabolism reported above and incubations were performed in triplicate.

**Cross species UGT and CYP metabolism profiling.** Mixed gender pooled HLM and pooled microsomes from males of 5 additional species (cynomolgus monkey, minipig, rat, mouse and dog)

DMD Fast Forward. Published on December 7, 2022 as DOI: 10.1124/dmd.122.001024
This article has not been copyedited and formatted. The final version may differ from this version.

were prepared and incubated under the same conditions as described above for both UGT and CYP experimental conditions. The experiments for all 5 animal species were performed in two replicates.

**Unbound fraction in microsomal incubations and human plasma.** Unbound fractions were determined in incubation media (1 mg/mL human liver microsomes and 1 mg/mL human liver microsomes supplemented with 2% w/v BSA) and undiluted human plasma. Equilibrium dialysis was performed against 133 mM phosphate buffer at pH 7.4, over 5 hours at 37 °C in a 5% $CO_2$ atmosphere, using a Teflon equilibrium dialysis plate (96-well, 150 µL, half-cell capacity) and cellulose membranes (12-14 kDa molecular weight cut-off) from HT-dialysis (Gales Ferry, Connecticut). Aliquots from the donor and receiver compartments were combined with buffer or blank plasma (or HLM) to make 10% (v/v) plasma (or HLM) matrix-matched samples. The samples were further prepared by the addition of acetonitrile-containing internal standard. Samples were kept on ice for 30 minutes, centrifuged at 6500g for 20 minutes and the supernatants removed for LC-MS/MS analysis.

**Blood to plasma partitioning.** Fresh blood was spiked with the test compound (1µM) and incubated (n=4) at 37°C in a 5% $CO_2$ environment for 1 hour. Aliquots of the blood were taken at the beginning (to enable checks for drug stability) and the end of the experiment. An aliquot of incubated blood was centrifuged to generate plasma. Performance of the blood/plasma partitioning experiment was monitored by the additional incubation of a positive control compound (chloroquine). The plasma and blood samples were matrix matched, mixed with acetonitrile (containing 50 ng/mL of tolbutamide as internal standard) and centrifuged. The supernatants were removed and analyzed by LC-MS/MS following appropriate dilution. The blood to plasma partitioning ratio (BPP) was determined as follows:

$$BPP = Peak\ Area\ Ratio\ (Blood)\ /\ Peak\ Area\ Ratio\ (Plasma) \quad (1)$$

DMD Fast Forward. Published on December 7, 2022 as DOI: 10.1124/dmd.122.001024
This article has not been copyedited and formatted. The final version may differ from this version.

where the peak area ratio values of the drug versus internal standard for the 1h incubated samples were used.

**LC-MS/MS analysis.** The LC-MS/MS system was comprised of two UHPLC pumps (Shimadzu LC-30AD), an autosampler (Shimadzu Nexera X2) and an API 6500 (AB-Sciex) mass spectrometer for the analysis of the samples from the metabolism assays. The samples for the blood to plasma patronizing were analyzed by LC-MS utilizing an API5000 mass spectrometer (AB Sciex) coupled to a UHPLC chromatography system. The chromatography conditions, analyte retention times and MS/MS analysis parameters are reported in the Supplementary Information, Tables S4 and S5.

**Data analysis.** The natural logarithm of the peak area ratios (test compound peak area/internal standard peak area) were plotted against time and the slope of the linear regression was determined using Microsoft Excel 2010 (Redmond, WA, US). The elimination rate constant (k) was calculated as:

$$k = (-slope) \quad (2)$$

Elimination rate constant determinations were performed using 8 timepoints from a single incubation lasting 30-45 minutes and using 1 mg/mL microsomal protein. With the ability to resolve 10% drug depletion, the limit of quantification was ~3 µL/min/mg. In order to resolve lower intrinsic clearance values, longer incubation times, higher measurement accuracy or more datapoints would be needed. Further resolution was obtained in this work by pooling the data from multiple incubations that had been performed and analyzed in parallel, and determining the drug elimination rate constant for the cohort of data as a whole. Such analyses were performed using Prism (version 8.4.2, GraphPad Software LLC) and resulted in an intrinsic clearance limit of quantification of 1 µL/min/mg with data uncertainty reported in terms of the 95% confidence interval limits.

The intrinsic clearance of UGTs and CYPs [$CL_{int}$ (µL/min/mg protein)] was calculated as:

DMD Fast Forward. Published on December 7, 2022 as DOI: 10.1124/dmd.122.001024
This article has not been copyedited and formatted. The final version may differ from this version.

$$CL_{int} = \frac{k*1000}{microsomal\ protein\ conc\ (mg/mL)} \qquad (3)$$

The total $CL_{int}$ (and similarly total $Cl_{int,u}$) was determined by summing the metabolic clearance from equation 4 in CYP and UGT (+BSA) metabolism conditions:

$$CL_{int} = CL_{int}(UGT) + CL_{int}(CYP) \quad (4)$$

The unbound intrinsic clearance [$CL_{int,u}$ (µL/min/mg protein)] was calculated for each incubation using the experimentally measured microsomal unbound fraction ($f_{u,mic}$):

$$CL_{int,u} = \frac{CL_{int}}{f_{u,mic}} \qquad (5)$$

The unbound intrinsic in vivo clearance in the liver $CL_{int,u}$ (µL/min/kg BW) was calculated by equation (6):

$$in\ vivo\ CL_{int,u} = \frac{CL_{int,u} \cdot MPPGL \cdot LW}{BW} \quad (6)$$

Where the microsomal protein per gram of liver (MPPGL) was 45 mg per gram of tissue (Barter et al., 2007), LW was the weight of the liver (1.8 kg) and BW the body weight (70 kg), and $fu_{inc}$ was the unbound fraction in the medium.

The hepatic plasma clearance ($CL_p$) was calculated from the well stirred model (Yang et al., 2007):

$$CL_b = \frac{Q_b\ in\ vivo\ CL_{int,u} \cdot f_{u,plasma}}{Q_b + in\ vivo\ CL_{int,u} \cdot f_{u,plasma}/\ BPP} (7)$$

where the $Q_b$ represented the blood flow rate of (23 mL/min/kg) (Kratochwil et al., 2017) and BPP is the blood plasma partitioning coefficient. Blood/plasma partitioning values were derived under the same experimental conditions which enabled direct comparison of binding for the enantiomers.

All graphs reported in this work were drawn using Prism v8.4.2 (GraphPad Software Inc., San Diego, CA).

In the absence of authentic standards for glucuronide metabolites, the enantioselectivity effects were estimated considering the rates of substrate depletion and the apparent relative appearance rates of the respective metabolite peaks in the LC-MS/MS analysis.

**Enantiomer structure overlays.** The molecular overlapping of each pair of enantiomers was performed using a ligand based-virtual screening by FLAP 2.2.1 (Molecular Discovery Ltd.). FLAP described the molecules with molecular interaction fields (MIFs). In this screening 4 probes were used: DRY (hydrophobic), H (shape), N1 (hydrogen bond donor), and hydrogen bond acceptor (O) and with a resolution of 0.75 Å. The molecules were uploaded with a maximum number of 25 conformers and using a root mean square conformer similarity of 0.30. The ligand based virtual screening was performed with optimized fit to template option and using two different approaches. The first used a constraint that limited the degrees of freedom of the molecules and forced both enantiomers to overlap at the position of conjugation. The second was performed without any constraint. Medetomidine enantiomers with two sites of conjugation were subject to a double constraint overlapping both sites of metabolism. The best score (best overlapping) was considered using GlobP molecular descriptors because it considers the contribution of hydrophobic, hydrogen bond donor, hydrogen bond acceptor, and shape.

DMD Fast Forward. Published on December 7, 2022 as DOI: 10.1124/dmd.122.001024
This article has not been copyedited and formatted. The final version may differ from this version.

## Results

*Stereoselective drug glucuronidation by HLM*

The stereoselectivity of medetomidine, RO5263397, propranolol and testosterone glucuronidation was assessed initially using a drug concentration of 1μM, mixed gender pooled HLM (supplemented with alamethicin to counter latency effects but without BSA addition) and optimized buffer conditions (Walsky et al., 2012; Badee et al., 2018). An 8.7-fold higher intrinsic clearance of levomedetomidine was observed in human liver microsomes compared with dexmedetomidine (drug depletion and glucuronide formation profiles shown in Figure 2, $CL_{int}$ data shown in Table 2). Even more strikingly, a >36-fold higher intrinsic clearance was observed for RO5263397 compared with its enantiomer RO5263396. This was mirrored by a 74-fold difference in the apparent relative rates of glucuronide formation, assuming equal LC-MS/MS responses for the glucuronides of the two molecules (Figure 2 and Supplemental Table 2). The intrinsic clearance of propranolol was very low, preventing comparison of intrinsic clearance values and calculation of a ratio. Apparent metabolite appearance rate was 6.6-fold higher for *S*-propranolol compared with *R*-propranolol. Epitestosterone was glucuronidated by HLM ~3-fold faster under these simple incubation conditions than its epimer testosterone. This initial experiment confirmed high stereoselectivity under combined hepatic UGT test conditions and the basis for follow-up studies.

*Protein binding and blood / plasma partitioning*

Protein binding was determined using undiluted human plasma, 1 mg/mL HLM and 1 mg/mL HLM supplemented with 2% w/v BSA to reflect in vivo and in vitro conditions (Table 3). BSA supplementation reduced medetomidine free fraction in HLM only slightly for both enantiomers, from ~51% to 32%. Levomedetomidine unbound plasma fraction was 21% compared with 14% for dexmedetomidine. No significant stereoselectivity in protein binding was seen for the RO5263397 enantiomers in HLM, HLM +BSA or plasma. *R*-propranolol showed a similar unbound fraction in

DMD Fast Forward. Published on December 7, 2022 as DOI: 10.1124/dmd.122.001024
This article has not been copyedited and formatted. The final version may differ from this version.

HLM in the absence and presence of BSA. For the *S* enantiomer a 2-fold lower unbound fraction was measured in the presence of BSA. Plasma protein binding for both propranolol enantiomers was similar, $f_u$ ~35%. Albani *et al* reported similar free fractions for both the propranolol enantiomers in human plasma, but lower actual values (11%-12%) whilst Walle *et al* reported values of 22%-25% (Walle et al., 1983; Albani et al., 1984). These reports suggest little enantiomeric binding preference over all in human plasma, despite differences in free fraction between studies and sensitivity to AGP binding being observed. Testosterone exhibited the largest protein binding effects: Supplementation of HLM with BSA reduced epitestosterone and testosterone unbound fractions substantially, from 63% to 12% and from 70% to 10%, respectively. These data were consistent with those previously reported (Badee et al., 2018). Testosterone free fraction in plasma was the lowest of any of the drugs tested (5-6%). Blood/plasma ratios were the same for the stereoisomers of medetomidine, RO5263397 and testosterone (Table 3). Propranolol showed some stereoselectivity with blood/plasma ratios of 0.74 ±0.06 and 1.16 ±0.09 for *S*- and *R*-propranolol, respectively.

*Effect of BSA on Glucuronidation by Human Liver Microsomes*

Metabolism experiments using pooled HLM were repeated in the presence and absence of 2% w/v BSA for all four enantiopairs (Figure 3, Table 2). Apparent (experimentally observed) medetomidine intrinsic clearances were not substantially affected by BSA presence, and even slightly reduced. Medetomidine unbound $CL_{int,u}$ values were slightly increased for both isomers in the presence of BSA (Supplemental Table 2). The apparent observed intrinsic clearance of RO5263397 was increased 2-fold in presence of BSA, whereas depletion of RO5263396 was still not measurable. (In addition, RO5263396-glucuronide formation was not increased by BSA addition.) RO5263397 and its enantiomer were not bound to BSA and therefore $CL_{int,u}$ did not significantly differ from the apparent $CL_{int}$ value (Supplemental Table 2). Apparent propranolol glucuronide appearance (Supplemental Table 2) was substantially enhanced by BSA (*S*-propranolol

DMD Fast Forward. Published on December 7, 2022 as DOI: 10.1124/dmd.122.001024
This article has not been copyedited and formatted. The final version may differ from this version.

by 7.6-fold and that for *R*-propranolol by 7.1-fold). *R*-propranolol $CL_{int}$ remained below the limit of quantification (< 1 μL/min/mg). In contrast, the *S* enantiomer had a low but measurable $CL_{int}$ of 3.4 μL/min/mg. Epitestosterone and testosterone were subject to both free fraction reduction (leading to lower turnover) and enzyme activity enhancement (leading to higher turnover) on addition of BSA. The apparent intrinsic clearance of epitestosterone was increased 1.7-fold and $CL_{int,u}$ increased 9-fold (Supplemental Table 2). In contrast, the apparent $CL_{int}$ for testosterone was approximately halved (Table 2) although the $CL_{int,u}$ increased 2.8-fold. Thus BSA increased the epitestosterone / testosterone $CL_{int}$ ratio from 3.4-fold to 14-fold (Supplemental Table 2).

*Activity of human kidney and intestinal microsomes and effect of BSA*

Pooled human kidney and intestinal microsomes (Table 2) did not measurably turn over RO5263397, medetomidine or propranolol due to either low expression of relevant enzymes (such as UGT2B10 and UGT1A4 for RO5263397 and medetomidine) or inherently low drug clearance via glucuronidation (propranolol). The presence of BSA increased the apparent glucuronide formation rate of *S*-propranolol by 5.0- and 12-fold for HIM, and HKM, respectively (Supplemental Table 3). For *R*-propranolol the increases were 6.5- and 12-fold for HIM, and HKM, respectively. The apparent glucuronide formation per milligram kidney microsomal protein was similar to liver. In contrast, little glucuronide formation and no BSA enhancement was seen using intestinal microsomes. A marked tissue difference was seen for epitestosterone and testosterone. Intestinal microsomes were ~4-fold more active in testosterone metabolism than liver microsomes (Table 2), both in the presence and absence of BSA. In contrast, intestinal microsomes were around 5-fold less active than liver microsomes in the metabolism of epitestosterone in the absence or presence of BSA. Kidney microsomes were highly active in epitestosterone glucuronidation but not active in testosterone glucuronidation. The presence of BSA increased the activity of epitestosterone of around 2-fold in HIM and HKM, but the $CL_{int}$ of testosterone in HIM was reduced more than 2-fold (Table 2).

DMD Fast Forward. Published on December 7, 2022 as DOI: 10.1124/dmd.122.001024
This article has not been copyedited and formatted. The final version may differ from this version.

*Differential CYP and UGT selectivity*

Oxidative metabolism of the drug molecules was examined by incubating with mixed gender pooled human liver microsomes in the presence of NADPH, with incubation conditions optimized for CYP activity, and comparing these data with incubations optimized for UGT activity. (Figure 4; intrinsic clearance data shown in Supplemental Table 1). Oxidative metabolism was slow, relative to glucuronidation, for levomedetomidine, dexmedetomidine, RO5263397, epitestosterone and testosterone but substantially more rapid for both *R*- and *S*-propranolol (Figure 3, Supplemental Table 1). RO5263396 was stable in both UGT and CYP metabolism experiments with intrinsic clearance below the limit of quantification (1 µL/min/mg).

When UGT-mediated and CYP-mediated intrinsic clearances were summed, the selectivity for levomedetomidine metabolism over that of dexmedetomidine was almost completely retained, as CYP metabolism was slow for both enantiomers in comparison with glucuronidation. Enantioselectivity for RO5263397 vs RO5263396 was >36-fold and both enantiomers were stable towards CYP metabolism (<1 µL/min/mg). Both enantiomers of propranolol were stable in glucuronidation experiments, although higher *S*-propranolol glucuronide formation was observed compared with that of *R*-propranolol (6.6-fold apparent ratio assuming an equal LC-MS/MS response for both glucuronide metabolites) (Supplemental Table 2). However, the opposite enantioselectivity and higher $CL_{int}$ values were observed under CYP metabolism conditions, with ~6-fold higher *R*-propranolol versus *S*-propranolol oxidation $CL_{int}$ (Figure 4). UGT metabolism favored epitestosterone turnover versus testosterone by around 3-fold. This ratio was relatively unaffected on combination with CYP $CL_{int}$ data as $CL_{int,UGT} > CL_{int,CYP}$ albeit with a slightly higher $CL_{int,CYP}$ for testosterone compared to that of epitestosterone (1.3-fold) (Supplemental Table 1).

*$CL_{int}$ ratio calculations and extrapolation*

DMD Fast Forward. Published on December 7, 2022 as DOI: 10.1124/dmd.122.001024
This article has not been copyedited and formatted. The final version may differ from this version.

In vitro to in vivo extrapolation (IVIVE) was performed to estimate the effect of metabolism stereoselectivity on the hepatic clearance. The in vivo hepatic intrinsic clearances and the hepatic clearance for each pair of enantiomers are reported in Table 4. The combined unbound intrinsic clearances in HLM from CYP and UGT metabolism experiments in presence of BSA were used. As the $f_{u,plasma}$ values for each enantiopair were very similar, there was little change in the ratio of intrinsic clearance when extrapolating from in vitro $CL_{int,u}$ to in vivo hepatic $CL_{int,u}$. Applying the well stirred model for hepatic metabolism, the hepatic clearance of levomedetomidine was predicted to be around 2.7-fold higher compared to dexmedetomidine. The CYP contribution to the total clearance of levomedetomidine was small (3%), whereas dexmedetomidine had a higher contribution of CYPs (~30 %). The predicted hepatic clearance of RO5263397 was >10 fold higher than that estimated for RO5263396, which was almost stable towards both UGT and CYP metabolism in vitro.

The hepatic intrinsic clearance of *R*-propranolol was 4.2-fold higher than that observed for *S*-propranolol (*S*/*R* ratio 0.24), and the corresponding predicted hepatic clearance was ~2-fold higher for the R enantiomer. CYP metabolism drove overall metabolism enantioselectivity due to the high turnover rates for CYPs compared with UGTs. Epitestosterone was calculated to have a higher hepatic intrinsic clearance (11-fold) compared to that estimated for testosterone, but only ~1.5-fold higher hepatic clearance due to hepatic blood flow limitations. Additional contributions from extrahepatic clearance, especially by glucuronidation in kidney and intestine, may also be important when considering overall drug clearance. These have not been assessed in this study due to limitations in scaling factor confidence (Ahmed et al., 2022).

*Species differences*

Pooled male donor microsomes from five preclinical species (CD-1 mouse, Wistar Han rat, beagle dog, Göttingen minipig and cynomolgus monkey) were tested in parallel with mixed gender pooled HLM using CYP and UGT metabolism conditions (Figure 4, Supplemental Table 1). The

DMD Fast Forward. Published on December 7, 2022 as DOI: 10.1124/dmd.122.001024
This article has not been copyedited and formatted. The final version may differ from this version.

substantial UGT-mediated levomedetomidine turnover and higher intrinsic clearance versus dexmedetomidine observed using HLM was not observed for the other species where $CL_{int}$ values were all below the limit of quantification (except for dog, >4-fold higher $CL_{int}$ in favor of levomedetomidine). Indeed, an opposite enantioselectivity in favor of dexmedetomidine of 3.2- and 2.2-fold was observed using CYP metabolism conditions for cynomolgus monkey and rat, respectively. Mouse, dog and minipig metabolism by CYPs suggested little enantioselectivity over all (<1.3-fold). Much higher human selective glucuronidation of RO5263397 compared with RO5263396 was seen, whereas none of the other species showed turnover of RO5263397, indicating that glucuronidation rates and metabolic pathways can be highly species dependent. Under oxidative metabolism conditions, RO5263396 was metabolized by cynomolgus, rat, mouse, and minipig liver microsomes with intrinsic clearance values ranging from 4.3 to 12 μL/min/mg, whereas RO5263397 was stable to oxidative metabolism in all species (Figure 4).

Propranolol was much more rapidly cleared by oxidative metabolism than by glucuronidation by all species microsomes, consistent with HLM. However, the enantioselectivity was not the same for all species. Cynomolgus and mouse showed the same selectivity for *R*-propranolol as human, but rat and minipig showed an opposite enantioselectivity, with higher turnover of *S*-propranolol. Finally, dog did not show significant enantioselectivity. Cynomolgus monkey liver microsomes showed higher selectivity towards epitestosterone glucuronidation (>6.2-fold) clearance than human (3.4-fold) and also showed preferential epitestosterone oxidation. The UGT selectivity towards epitestosterone was reversed in dog (25-fold in favor of testosterone). Dog microsomal oxidative $CL_{int}$ was 3.4-fold higher for epitestosterone and 6.6-fold lower for testosterone compared with UGT $CL_{int}$ (Figure 4 and Supplemental Table 1). Rat and mouse liver microsomes also exhibited the opposite enantioselectivity to that of HLM in presence of UDPGA. However, this was overshadowed by a more rapid oxidative clearance for rat and mouse of up to >50-fold and 6.7-fold for epitestosterone and testosterone, respectively (Supplemental Table 1).

DMD Fast Forward. Published on December 7, 2022 as DOI: 10.1124/dmd.122.001024
This article has not been copyedited and formatted. The final version may differ from this version.

*Molecular modelling and stereoisomer similarity*

The ligand based virtual screening overlays shown in Figure 5 give a three dimensional representation of the similarity of the respective enantiomers. In the constrained condition the site of glucuronidation (indicated with arrows) was forced to overlap, highlighting non-superimposable elements of the structures, which may have affected metabolism-capable binding poses within enzyme active sites. For RO5263396/7 the oxazole scaffold was fully overlapped for both enantiomers, but the substituents in the aromatic scaffold were non-superimposable. Propranolol enantiopairs overlapped well for the aromatic scaffold, but the overlay of the isopropyl amino group was not optimal. Testosterone and epitestosterone showed a high degree of alignment, but with a slight difference of the ketone group. For comparison, the unconstrained molecular overlays are also shown giving an impression of 3D feature similarity.

## Discussion

The individual enzyme glucuronidation stereoselectivity of medetomidine, propranolol, and testosterone were collected from published reports and are summarized in Table 1. (Additional data for RO5263397 and RO5263396 are shown in Supplemental Figure 1 and associated information). In some reports the overall UGT enantioselectivity was assessed, typically using HLM without BSA supplementation. However, extrapolation to the in vivo situation has not typically been possible due to differential impacts of BSA on different drug molecules and UGT isoforms, the lack of non-UGT metabolism data for some compounds, and the absence of relative activity factors for the recombinantly expressed UGTs. In addition, microsomal UGT activities are affected by many factors including buffer type, the presence of detergent or pore-forming agents and concentrations of metal ions and cofactors (Walsky et al., 2012; Badee et al., 2018). The in vitro conditions used in our study were selected for optimal UGT metabolism rate assessment (or optimal CYP metabolism in those experiments), which occurred under different buffer and preparation conditions. The

DMD Fast Forward. Published on December 7, 2022 as DOI: 10.1124/dmd.122.001024
This article has not been copyedited and formatted. The final version may differ from this version.

current study therefore set out to make an as good as possible assessment using currently available methodologies of the overall effect of individual UGT enantioselectivity on hepatic clearance.

*Medetomidine*

Kaivosaari *et al* (Kaivosaari et al., 2008) reported the involvement of UGT2B10 as the high affinity enzyme mainly involved in the metabolism of both levomedetomidine and dexmedetomidine but with higher intrinsic clearance of levomedetomidine. Dexmedetomidine is the active drug moiety and is also a highly selective UGT2B10 substrate (Milani et al., 2020), even though turnover was significantly less than that observed for levomedetomidine (Supplemental Figure 1). From the reported HLM kinetics data, glucuronidation intrinsic clearance values of ~150 and ~25 µL/min/mg were estimated for levomedetomidine and dexmedetomidine, respectively, which were in close agreement with values from this study. The 6-fold higher intrinsic clearance for levomedetomidine was similar to the ~ 8.5-fold enantioselectivity observed in the present study. The high stability of both compounds in HIM and HKM was explained by the involvement of UGT2B10 and its much higher expression in the liver compared to the intestine and kidney (Jones and Lazarus, 2014). Medetomidine showed high liver UGT-dependent intrinsic clearance, no substantial enantiomeric difference in protein binding and a low CYP-dependent intrinsic clearance. These factors meant that the 9-fold difference in HLM UGT intrinsic clearance was carried forward to make a 6-fold difference extrapolated hepatic intrinsic clearance (Table 4). Applying the well-stirred model to account for liver blood flow, this predicted clearance ratio was diminished to 2.7-fold due to higher effect of blood flow limitation for levomedetomidine compared with dexmedetomidine. Preclinical species would not have enabled prediction to human due to species differences in both glucuronidation contribution to metabolism and enantioselectivity: In all tested species the oxidative intrinsic clearance was much higher as a proportion of total metabolism and none of the other species showed the human selectivity towards high UGT2B10-mediated levomedetomidine glucuronidation.

DMD Fast Forward. Published on December 7, 2022 as DOI: 10.1124/dmd.122.001024
This article has not been copyedited and formatted. The final version may differ from this version.

*RO5263397*

RO5263397 displayed a metabolism profile similar to levomedetomidine but with somewhat higher metabolic stability and a greater extent of UGT2B10 selectivity (Badée et al., 2019; Milani et al., 2020; Takahashi et al., 2021). The intrinsic clearance of RO5263397 versus enantiomer RO5263396 was at least 36-fold higher. Unfortunately, the active enantiomer RO5263397 displayed the less favorable characteristic of high human-specific UGT2B10-mediated intrinsic clearance, whereas enantiomer RO5263396 had lower intrinsic clearance and a more balanced profile of UGT1A4, UGT2B10 and some CYP-mediated clearance. The addition of BSA increased the glucuronidation rate of RO5263397 ~2-fold, confirming that BSA can enhance UGT2B10 activity (Walsky et al., 2012; Pattanawongsa et al., 2016). Similarly to medetomidine, both enantiomers were stable in HIM and HKM experiments and so extrahepatic clearance is not expected to contribute substantially. The animal models substantially under-represented human UGT metabolism of RO5263397, which highlighted their limitations for prediction of human metabolic clearance, metabolism pathways and enantioselectivity. Although UGT2B10 activity showed high stereoselectivity in medetomidine and RO5263397 metabolism, the available literature is too limited to state that UGT2B10 is more likely to exhibit stereoselective drug metabolism compared to other UGT isoforms.

*Propranolol*

Propranolol is glucuronidated by UGTs 1A1, 1A9, 1A10, 2B4, 2B7 and 2B17 and each enzyme displayed a different level of enantioselectivity (Table 1) (Sten et al., 2006; Hanioka et al., 2008; Yu et al., 2010). Sten et al (Sten et al., 2009) described the differential enantioselectivity of UGT1A9 and UGT1A10 towards propranolol glucuronidation indicating that the HLM and HKM preference for *S*-propranolol glucuronidation is likely driven by UGT1A9. This was also observed in the present study where human liver and kidney microsomes showed the highest metabolism, consistent with high UGT1A9 expression in the kidney and liver (Mukai et al., 2014). As expected, BSA

DMD Fast Forward. Published on December 7, 2022 as DOI: 10.1124/dmd.122.001024
This article has not been copyedited and formatted. The final version may differ from this version.

enhanced *S*-propranolol glucuronidation substantially in HLM and HKM but not to the same extent in HIM (Supplementary Table 3). These data were also consistent with the known enhancement of UGT1A9 by addition of BSA (Rowland et al., 2008; Manevski et al., 2011). *R*-propranolol was metabolized more by HLM than HIM and HKM (Figure 3). There was a high BSA effect (~ 7-fold higher metabolism in the HLM, ~6.5-fold in HIM and 12-fold in HKM), likely related to the activity of UGT2B7 (Manevski et al., 2011) (Supplemental Table 3). *R*-propranolol had higher clearance in vivo and lower circulating levels of glucuronide (Silber et al., 1982; Olanoff et al., 1984). Propranolol enantioselectivity differences were therefore informative for the understanding of UGT enzyme specificity, but were not reflected in the in vivo situation due to higher oxidative metabolism. The predicted in vivo hepatic unbound intrinsic clearance enantioselectivity of propranolol was around 4.2 in favor of the R enantiomer. However, taking into account blood / plasma partitioning and hepatic blood flow, the hepatic clearance ratio was slightly lower (~2-fold) and was in accordance with the systemic clearance reported by Olanoff et al., which was on average 1.2 in favor of *R*-propranolol in a study with 5 subjects (Olanoff et al., 1984). This comparison was encouraging, especially considering that the present study focused on incubation conditions without enzyme saturation, whereas partial saturation of metabolism is observed at the different doses of propranolol investigated (Silber et al., 1982).

*Testosterone*

The role of UGTs 2B7 and 2B17 in the selective metabolism of epitestosterone and testosterone, respectively, was previously described in the context of anabolic steroid misuse testing by Sten *et al* (Sten et al., 2009). The differential enzyme involvement was especially evident in the tissue selectivity experiments of the present study (high epitestosterone $CL_{int}$ by kidney microsomes, compared with low testosterone $CL_{int}$ likely due to high UGT2B7, but low UGT2B17 expression in the kidney) and effect of BSA (epitestosterone turnover by UGT2B7 activated more than testosterone turnover by UGT2B17; Figure 3). The increase of the unbound epitestosterone

DMD Fast Forward. Published on December 7, 2022 as DOI: 10.1124/dmd.122.001024
This article has not been copyedited and formatted. The final version may differ from this version.

metabolism in presence of BSA (~9-fold) was in accordance with what observed for UGT2B7 using the probe substrate zidovudine (around 10-fold higher in presence of BSA) (Walsky et al., 2012). The lower effect of BSA on testosterone turnover (e.g. by UGT2B17) was consistent with previous reports (Badée et al., 2018) and for other UGT2B17 substrates (Manevski et al., 2013). Testosterone is frequently used in vitro as a selective substrate of CYP3A4 for drug-drug interaction and enzyme phenotyping experiments using CYP-selective metabolism conditions (Walsky and Obach, 2004; Bohnert et al., 2016). However, as glucuronidation in the absence of BSA is significantly faster than oxidation by HLM (~7.5-fold), testosterone clearance in the liver is likely more dependent on conjugation than oxidation. The five animal models tested were unable to reproduce the human stereoselectivity observed in either glucuronidation or overall metabolism.

*Visualization of the different enantiomers and concluding remarks*

A ligand based-virtual screening was used to visualize the similarity of the enantiomers and identify the potential groups which may cause the in the UGT metabolism stereoselectivity. Very similar molecular overlapping, in particular under the constrained screening setting, suggesting that quite subtle binding interaction changes may confer enantiomer selectivity. For instance, medetomidine and RO5263397/6 enantiomer structures are almost completely superimposable (Figure 5), with the exception of the methyl group on the medetomidine bridging methylene moiety and the ortho substituents of the RO5263397/6 phenyl ring. The low molecular weight, moderate lipophilicity and moderate-high permeability of these drugs is likely to result in low CYP and transporter contribution to drug clearance and therefore a high impact of the high affinity UGT, in this case UGT2B10. The extreme sensitivity of UGT2B10 metabolism to stereoisomerism suggests some quite specific drug binding interactions.

We conclude that for drugs such as medetomidine and RO5263397 the high individual UGT contribution to conjugation, lack of additional metabolism routes and absence of stereoselective protein binding are likely to result in high in vivo clearance stereoselectivity. For some drugs that

exhibit high extrahepatic metabolism the overall drug clearance calculations may need to consider the contributions of other organs such as kidney and intestine. The establishment and validation of relevant scaling factors for these tissues will be an important next step towards their inclusion in clearance prediction work (Docci et al., 2020; Ahmed et al., 2022).

DMD Fast Forward. Published on December 7, 2022 as DOI: 10.1124/dmd.122.001024
This article has not been copyedited and formatted. The final version may differ from this version.

**Acknowledgments**

The authors thank Fidelta Ltd (Zagreb, Croatia) for performance under contract of protein binding experiments and Unilabs York Bioanalytical Solutions (Sandwich, UK) for performance of blood/plasma partitioning experiments. We kindly acknowledge helpful feedback on this manuscript from Neil Parrott (Hoffmann-La Roche, Basel, CH). We also thank Drs. Franz Schuler, Adrian Roth (Hofmann-La Roche, Basel, CH), and Professor Gabriele Cruciani (University of Perugia) for sponsoring this project.



**Authorship Contributions**

Participated in research design: Milani, Qiu, Fowler.

Conducted experiments: Milani, Qiu.

Performed data analysis: Milani, Qiu, Fowler.

Contributed to the writing of the manuscript: Milani, Fowler.

DMD Fast Forward. Published on December 7, 2022 as DOI: 10.1124/dmd.122.001024
This article has not been copyedited and formatted. The final version may differ from this version.

# References

Agranat I, Wainschtein SR, and Zusman EZ (2012) The predicated demise of racemic new molecular entities is an exaggeration. *Nature Reviews Drug Discovery* **11:**972-973.

Ahmed AN, Rostami-Hodjegan A, Barber J, and Al-Majdoub ZM (2022) Examining Physiologically Based Pharmacokinetic Model Assumptions for Cross-Tissue Similarity of Activity per Unit of Enzyme: The Case Example of Uridine 5'-Diphosphate Glucuronosyltransferase. *Drug Metab Dispos* **50:**1119-1125.

Albani F, Riva R, Contin M, and Baruzzi A (1984) Stereoselective binding of propranolol enatiomers to human a1-acid glycoprotein and human plasma. *British Journal of Clinical Pharmacology* **18:**244-246.

Badée J, Fowler S, de Wildt SN, Collier AC, Schmidt S, and Parrott N (2018) The Ontogeny of UDP-glucuronosyltransferase Enzymes, Recommendations for Future Profiling Studies and Application Through Physiologically Based Pharmacokinetic Modelling. *Clinical Pharmacokinetics*.

Badée J, Qiu N, Collier AC, Takahashi RH, Forrest WF, Parrott N, Schmidt S, and Fowler S (2019) Characterization of the ontogeny of hepatic UDP-glucuronosyltransferase enzymes based on glucuronidation activity measured in human liver microsomes. *The Journal of Clinical Pharmacology* **59:**S42-S55.

Badee J, Qiu N, Parrott NJ, Collier AC, Schmidt S, and Fowler S (2018) Optimization of Experimental Conditions of Automated Glucuronidation Assays in Human Liver Microsomes using a Cocktail Approach and Ultra-High Performance Liquid Chromatography-Tandem Mass Spectrometry. *Drug Metabolism and Disposition***:**dmd.118.084301.

Barter ZE, Bayliss MK, Beaune PH, Boobis AR, Carlile DJ, Edwards RJ, Brian Houston J, Lake BG, Lipscomb JC, and Pelkonen OR (2007) Scaling factors for the extrapolation of in vivo metabolic drug clearance from in vitro data: reaching a consensus on values of human micro-somal protein and hepatocellularity per gram of liver. *Current drug metabolism* **8:**33-45.

Bohnert T, Patel A, Templeton I, Chen Y, Lu C, Lai G, Leung L, Tse S, Einolf HJ, and Wang Y-H (2016) Evaluation of a new molecular entity as a victim of metabolic drug-drug interactions—an industry perspective. *Drug Metabolism and Disposition* **44:**1399-1423.

Calcaterra A and D'Acquarica I (2018) The market of chiral drugs: Chiral switches versus de novo enantiomerically pure compounds. *Journal of pharmaceutical and biomedical analysis* **147:**323-340.

Coelho MM, Fernandes C, Remião F, and Tiritan ME (2021) Enantioselectivity in Drug Pharmacokinetics and Toxicity: Pharmacological Relevance and Analytical Methods. *Molecules* **26:**3113.

Davies NM (1995) Clinical pharmacokinetics of flurbiprofen and its enantiomers. *Clinical pharmacokinetics* **28:**100-114.

Docci L, Umehara K, Krahenbuhl S, Fowler S, and Parrott N (2020) Construction and Verification of Physiologically Based Pharmacokinetic Models for Four Drugs Majorly Cleared by Glucuronidation: Lorazepam, Oxazepam, Naloxone, and Zidovudine. *AAPS J* **22:**128.

Fowler S, Kletzl H, Finel M, Manevski N, Schmid P, Tuerck D, Norcross RD, Hoener MC, Spleiss O, and Iglesias VA (2015) A UGT2B10 splicing polymorphism common in african populations may greatly increase drug exposure. *Journal of Pharmacology and Experimental Therapeutics* **352:**358-367.

Hanioka N, Hayashi K, Shimizudani T, Nagaoka K, Koeda A, Naito S, and Narimatsu S (2008) Stereoselective glucuronidation of propranolol in human and cynomolgus monkey liver microsomes: role of human hepatic UDP-glucuronosyltransferase isoforms, UGT1A9, UGT2B4 and UGT2B7. *Pharmacology* **82:**293-303.

Jones NR and Lazarus P (2014) UGT2B gene expression analysis in multiple tobacco carcinogen-targeted tissues. *Drug Metabolism and Disposition* **42:**529-536.

Kaivosaari S, Toivonen P, Aitio O, Sipilä J, Koskinen M, Salonen JS, and Finel M (2008) Regio-and stereospecific N-glucuronidation of medetomidine: the differences between UDP glucuronosyltransferase (UGT) 1A4 and UGT2B10 account for the complex kinetics of human liver microsomes. *Drug Metabolism and Disposition* **36:**1529-1537.

Kratochwil NA, Meille C, Fowler S, Klammers F, Ekiciler A, Molitor B, Simon S, Walter I, McGinnis C, and Walther J (2017) Metabolic profiling of human long-term liver models and hepatic clearance predictions from in vitro data using nonlinear mixed-effects modeling. *The AAPS journal* **19:**534-550.

Manevski N, Moreolo PS, Yli-Kauhaluoma J, and Finel M (2011) Bovine serum albumin decreases Km values of human UDP-glucuronosyltransferases 1A9 and 2B7 and increases Vmax values of UGT1A9. *Drug metabolism and disposition* **39:**2117-2129.

Manevski N, Troberg J, Svaluto-Moreolo P, Dziedzic K, Yli-Kauhaluoma J, and Finel M (2013) Albumin stimulates the activity of the human UDP-glucuronosyltransferases 1A7, 1A8, 1A10, 2A1 and 2B15, but the effects are enzyme and substrate dependent. *PLoS One* **8:**e54767.

Milani N, Qiu N, Molitor B, Badée J, Cruciani G, and Fowler S (2020) Use of Phenotypically Poor Metabolizer Individual Donor Human Liver Microsomes To Identify Selective Substrates of UGT2B10. *Drug Metabolism and Disposition* **48:**176-186.

Mukai M, Tanaka S, Yamamoto K, Murata M, Okada K, Isobe T, Shigeyama M, Hichiya H, and Hanioka N (2014) In vitro glucuronidation of propofol in microsomal fractions from human liver, intestine and kidney: tissue distribution and physiological role of UGT1A9. *Die Pharmazie-An International Journal of Pharmaceutical Sciences* **69:**829-832.

Olanoff LS, Walle T, Walle UK, Cowart TD, and Gaffney TE (1984) Stereoselective clearance and distribution of intravenous propranolol. *Clinical Pharmacology & Therapeutics* **35:**755-761.

Pattanawongsa A, Nair PC, Rowland A, and Miners JO (2016) Human UDP-glucuronosyltransferase (UGT) 2B10: validation of cotinine as a selective probe substrate, inhibition by UGT enzyme-selective inhibitors and antidepressant and antipsychotic drugs, and structural determinants of enzyme inhibition. *Drug metabolism and disposition* **44:**378-388.

Rowland A, Elliot DJ, Knights KM, Mackenzie PI, and Miners JO (2008) The "albumin effect" and in vitro-in vivo extrapolation: sequestration of long-chain unsaturated fatty acids enhances phenytoin hydroxylation by human liver microsomal and recombinant cytochrome P450 2C9. *Drug metabolism and disposition* **36:**870-877.

Silber B, Holford NH, and Riegelman S (1982) Stereoselective disposition and glucuronidation of propranolol in humans. *J Pharm Sci* **71:**699-704.

Sten T, Bichlmaier I, Kuuranne T, Leinonen A, Yli-Kauhaluoma J, and Finel M (2009) UDP-glucuronosyltransferases (UGTs) 2B7 and UGT2B17 display converse specificity in testosterone and epitestosterone glucuronidation, whereas UGT2A1 conjugates both androgens similarly. *Drug Metabolism and Disposition* **37:**417-423.

Sten T, Qvisen S, Uutela P, Luukkanen L, Kostiainen R, and Finel M (2006) Prominent but reverse stereoselectivity in propranolol glucuronidation by human UDP-glucuronosyltransferases 1A9 and 1A10. *Drug metabolism and disposition* **34:**1488-1494.

Takahashi RH, Forrest WF, Smith AD, Badee J, Qiu N, Schmidt S, Collier AC, Parrott N, and Fowler S (2021) Characterization of Hepatic UDP-Glucuronosyltransferase Enzyme Abundance-Activity Correlations and Population Variability Using a Proteomics Approach and Comparison with Cytochrome P450 Enzymes. *Drug Metab Dispos* **49:**760-769.

Walle UK, Walle T, Bai SA, and Olanoff LS (1983) Stereoselective binding of propranolol to human plasma, alpha 1-acid glycoprotein, and albumin. *Clin Pharmacol Ther* **34:**718-723.

Walsky RL, Bauman JN, Bourcier K, Giddens G, Lapham K, Negahban A, Ryder TF, Obach RS, Hyland R, and Goosen TC (2012) Optimized assays for human UDP-glucuronosyltransferase (UGT) activities: altered alamethicin concentration and utility to screen for UGT inhibitors. *Drug Metab Dispos* **40:**1051-1065.

Walsky RL and Obach RS (2004) Validated assays for human cytochrome P450 activities. *Drug Metab Dispos* **32:**647-660.

Wang H, Yuan L, and Zeng S (2011) Characterizing the effect of UDP-glucuronosyltransferase (UGT) 2B7 and UGT1A9 genetic polymorphisms on enantioselective glucuronidation of flurbiprofen. *Biochemical pharmacology* **82:**1757-1763.

Yang J, Jamei M, Yeo KR, Rostami-Hodjegan A, and Tucker GT (2007) Misuse of the well-stirred model of hepatic drug clearance. *Drug Metabolism and Disposition* **35:**501-502.

Yu L, Qian M, Liu Y, Yao T, and Zeng S (2010) Stereoselective metabolism of propranolol glucuronidation by human UDP-glucuronosyltransferases 2B7 and 1A9. *Chirality* **22:**456-461.

## Footnotes

## Funding

This work was funded by F. Hoffmann - La Roche Ltd, Basel, Switzerland.

## Declaration of interest

The authors have no conflicts of interest to declare.

## Reprint Requests

Stephen Fowler, Ph.D.

Pharmaceutical Sciences, Roche Pharmaceutical Research and Early Development, Grenzacherstrasse 124, CH-4070 Basel, Switzerland.

E-mail: stephen.fowler@roche.com

DMD Fast Forward. Published on December 7, 2022 as DOI: 10.1124/dmd.122.001024
This article has not been copyedited and formatted. The final version may differ from this version.

**Legends for Figures**

**Figure 1. A) Molecular structures of the three enantiopairs and the epimers testosterone and epitestosterone tested in this work. The arrow indicates the site of metabolism and asterisk indicates location of the relevant stereocenter. For the epimers the asterisk highlights the unique different chiral center between testosterone and epitestosterone. B) Schematic representation of the experimental workflow and the in vitro – in vivo clearance extrapolation.**

**Figure 2. UGT-mediated drug depletion and metabolite formation of medetomidine, RO5263397, propranolol and testosterone and their enantiomers by pooled HLM**

Assessment of drug depletion (left hand graphs) and glucuronide metabolite formation (right hand graphs) for enantiopairs levo-/dex-medetomidine, RO5263397/RO5263396, S-/R-propranolol and epitestosterone/testosterone by pooled human liver microsomes supplemented with UDPGA. Medetomidine metabolite appearance profiles show sum of glucuronide metabolite signals. Data are mean ±SD from triplicate incubations performed in a preliminary experiment in the absence of BSA. Exponential decay profile fitted to drug depletion data and hyperbolic metabolite appearance profile fitted to glucuronide formation data. Red profiles / filled circles: faster metabolized enantiomer; black profiles / filled diamonds: slower metabolized enantiomer.

**Figure 3. Comparison of UGT-Mediated Human Tissue Microsomal Substrate Depletion Enantioselectivity HLM/HIM/HKM activities in the presence and absence of BSA:** Effect of BSA on human liver, kidney and intestinal microsomal glucuronidation activities. Mean data ±SD from four incubations performed in parallel are plotted with exponential decay profiles fitted to the drug depletion data. Black circles: HLM, red triangles: HIM, blue diamonds: HKM. Hollow symbols denote BSA supplementation. Inset figures show glucuronide metabolite LC-MS/MS peak area ratios. BSA supplementation enhanced metabolite generation by the following factors: *S*-

DMD Fast Forward. Published on December 7, 2022 as DOI: 10.1124/dmd.122.001024
This article has not been copyedited and formatted. The final version may differ from this version.

propranolol/HLM 7.6, *S*-propranolol/HIM 5.0, *S*-propranolol/HKM 12, *R*-propranolol/HLM 7.1, *R*-propranolol/HIM 6.5, *R*-propranolol/HKM 12 (Supplemental Table 3).

**Figure 4. Enantioselectivity of UGT- and CYP-Mediated Metabolism by Human and Different Preclinical Species Liver Microsomes**: Mean intrinsic clearance ±range of duplicate determinations shown. Note: The gray and red dotted line represent the BLQ (1 µL/min/mg protein) and the upper limit of quantification (1000 µL/min/mg protein), respectively. Incubations performed in the absence of BSA. Red bars: higher UGT turnover stereoisomers (RO5263397, levomedetomidine, S-propranolol, and epitestosterone), black bars: lower UGT turnover stereoisomers (RO5263396, dexmedetomidine, R-propranolol, and testosterone).

**Figure 5**. **Molecular overlapping of each pair of stereoisomers in unconstrained and constrained (site of metabolism forced to overlap) conditions**: Unconstrained and constrained molecular overlapping of each pair of stereoisomers. In red are shown the higher UGT turnover enantiomers (RO5263397, levomedetomidine, S-propranolol, and epitestosterone) and shown in black are the lower UGT turnover enantiomers RO5263396, dexmedetomidine, R-propranolol, and testosterone. Arrows and asterisks indicate the sites of conjugation (in the constrained poses) and the chiral centers, respectively. For the epimers testosterone and epitestosterone the asterisk represents only the unique different chiral center.

DMD Fast Forward. Published on December 7, 2022 as DOI: 10.1124/dmd.122.001024
This article has not been copyedited and formatted. The final version may differ from this version.

**Table 1. Reported Enantioselectivity of medetomidine, propranolol, testosterone-epitestosterone, and RO5263397/6 metabolism by UGTs.**

| Drug | Class compound | Administration | Metabolism Enzymes | | Enantioselectivity[a] | In vitro ref |
|---|---|---|---|---|---|---|
| | | | Major | Minor | | |
| Levomedetomidine/ Dexmedetomidine | $\alpha_2$-adrenergic agonist | Pure enantiomer | UGTs | | UGT2B10 (7.2) [b]<br>UGT1A4 (0.19) [b]<br>UGT1A3 (0.49)[b]<br>UGT2B7 (0.38)[b]<br>HLM (6.1)[b] | (Kaivosaari et al., 2008) |
| (S)-Propranolol/ (R)-Propranolol | β-adrenergic blocking agent | Racemate | CYPs | UGTs | UGT1A1 (2)[b]<br>UGT1A9 (11)<br>UGT1A10 (0.24)<br>UGT2B4(1.4)<br>UGT2B7 (0.79)<br>UGT2B17 (3.4) | (Sten et al., 2006) |
| | | | | | UGT1A9 (6.5)<br>UGT2B7 (0.8) | (Wang et al., 2011) |
| | | | | | HLM (1.1)<br>UGT1A9 (9.4)<br>UGT2B4 (1.9)<br>UGT2B7 (0.7) | (Hanioka et al., 2008) |
| Epitestosterone/ Testosterone[a] | Endogenous hormone | Endogenous compound | UGTs | CYPs | UGT2B17(ND epitestosterone)<br>UGT2B7(68)<br>UGT2A1(0.68) | (Sten et al., 2009) |
| RO5263397/ RO5263396 | Neuroscience | Pure enantiomer (RO5263397) | UGTs | | UGT2B10 (>12)[c]<br>UGT1A4 (1.5)[c] | See supplementary information |

[a] The metabolism rate ratios are shown in brackets. Testosterone and Epitestosterone are two epimers which have opposite configuration at the stereogenic center 1 from IUPAC nomenclature.

[b] $CL_{int}$ calculated as sum of $v_{max}/K_M$ for each metabolite formed.

[c]Ratio expressed as glucuronide formation due to the lack of depletion of RO5263396 in the UGT2B10 incubation and of both enantiomers in the UGT1A4, which was below the limit of quantification of $CL_{int}$ < 3 µL/min/mg. In the absence of authentic metabolite standards the MS/MS response was assumed to be the same for both the glucuronide metabolites.

ND: not determined as conjugation of epitestosterone could not be detected

**Table 2: Enantioselectivity of UGT-mediated metabolism in vitro using pooled human liver, intestine and kidney microsomes and effect of BSA supplementation. The values reported the apparent $CL_{int}$.**

| Compound | | Medetomidine | | | RO5263397/6 | | | Propranolol | | | Testosterone | | |
|---|---|---|---|---|---|---|---|---|---|---|---|---|---|
| | | Levo | Dex | Ratio | RO5263397 | RO5263396 | Ratio | S | R | Ratio | Epi | Test | Ratio |
| Tissue | | µL/min/mg | | | µL/min/mg | | | µL/min/mg | | | µL/min/mg | | |
| Liver | -BSA | 120 ±9 | 14 ±2 | 8.6 | 36 ±1 | BLQ | > 36 | BLQ | BLQ | ND | 353 ±5 | 105 ±4 | 3.4 |
| | +BSA | 96 ±5 | 11 ±2 | 8.7 | 68 ±2 | BLQ | >68 | 3.4 ±0.8 | BLQ | >3.4 | 597 ±28 | 43 ±2 | 14 |
| Intestine | -BSA | BLQ | BLQ | BLQ | BLQ | BLQ | BLQ | BLQ | BLQ | BLQ | 64 ±3 | 468 ±16 | 0.14 |
| | +BSA | BLQ | BLQ | BLQ | BLQ | BLQ | BLQ | BLQ | BLQ | BLQ | 112 ±8 | 191 ±7 | 0.59 |
| Kidney | -BSA | BLQ | BLQ | BLQ | BLQ | BLQ | BLQ | BLQ | BLQ | BLQ | 407±17 | BLQ | BLQ |
| | +BSA | BLQ | BLQ | BLQ | BLQ | BLQ | BLQ | BLQ | BLQ | BLQ | 817 ±33 | BLQ | BLQ |

BLQ: not determined since the $CL_{int}$ was below the limit of quantification (1µL/min/mg)

Notes: Additional information with the respective unbound CLs and their comparison between enantiomers are reported in the Supplementary Information in Table 2 and the propranolol glucuronide formation data in the Supplemental Table 3.

**Table 3: Protein Binding and Blood / Plasma Ratios**

| Test Compound | Protein Binding: Free Fraction (%) | | | Blood to Plasma Ratio |
|---|---|---|---|---|
| | HLM (1 mg/mL) | HLM (1 mg/mL) + BSA (2% w/v) | Human Plasma | |
| Levo-Medetomidine | 51 ±3 | 32 ±2 | 21.2 ±0.4 | 0.80 ±0.02 |
| Dex-Medetomidine | 53 ±3 | 32 ±2 | 14 ±1 | 0.71 ±0.02 |
| RO5263397 | 68 ±3 | 68 ±4 | 58 ±3 | 1.38 ±0.09 |
| RO5263396 | 71 ±10 | 73 ±9 | 53 ±1 | 1.30 ±0.05 |
| (S)-Propranolol | 39 ±1 | 21 ±1 | 32.6 ±0.4 | 0.74±0.06 |
| (R)-Propranolol | 39 ±3 | 42 ±1 | 37 ±2 | 1.16±0.09 |
| Epitestosterone | 63 ±2 | 11.9 ±0.3 | 5.7 ±0.2 | 0.64±0.04 |
| Testosterone | 70 ±6 | 10 ±1 | 4.9 ±0.2 | 0.69±0.01 |

All compounds tested at initial concentration of 1 μM in the protein-containing side of dialysis system. Values are mean ±SD from triplicate and quadruplicate determinations for the protein binding and the blood to plasma ratio, respectively. Hematocrit value was 0.48.

**Table 4: Extrapolation of Enantioselective intrinsic clearance from in vitro to in vivo**

| Compound | HLM (Unbound $CL_{int}$) UGT[a,b] | HLM (Unbound $CL_{int}$) CYP[a,b] | Summed [a] | Predicted in vivo clearance Hepatic unbound intrinsic clearance $CL_{int}$ | Predicted in vivo clearance Hepatic clearance $CL_p$ |
|---|---|---|---|---|---|
| | µL/min/mg | | | mL/min/kg | |
| Levomedetomidine | 300 ± 19 | 9.0 ± 6.5 | 309 ± 20 | 358 ± 25 | 14.8 ± 0.2 |
| Dexmedetomidine | 34 ± 6 | 16 ± 4 | 50 ± 7 | 58 ± 8 | 5.4± 0.5 |
| Ratio | 8.7 | 0.57 | 6.1 | 6.2 | 2.7 |
| RO5263397 | 100 ± 3 | <1.5 | 100 ± 3 | 116 ± 3 | 20.9 ± 0.1 |
| RO5263396[c] | <1.4 | <1.4 | <2.8 | < 3.2 | < 2.0 |
| Ratio | >73 | - | > 36 | > 36 | > 10 |
| S-Propranolol | 16 ± 1 | 46 ± 6 | 62 ± 7 | 72 ± 7 | 9.9 ± 0.4 |
| R-Propranolol | <2.4 | 271 ±22 | 271 ± 22 | 314± 25 | 21.7 ± 0. 3 |
| Ratio | >7.5 | 0.17 | 0.24 | 0.24 | 0.45 |
| Epitestosterone | 5012 ± 235 | 92 ± 5 | 5014 ± 240 | 5907 ± 277 | 14.11 ± 0.01 |
| Testosterone | 424 ± 20 | 20 ± 2 | 444 ± 22 | 514 ± 25 | 9.7 ± 0.2 |
| Ratio | 12 | 4.6 | 11 | 12 | 1.5 |

Extrapolation of Enantioselective intrinsic clearance from in vitro to in vivo. Unbound clearance in the HLM in presence of UDPGA and NADPH and their respective summed data for medetomidine, RO5263397/6, propranolol, and testo/epitestosterone. The summed clearances were applied to predict the in vivo clearance as unbound hepatic intrinsic clearance and hepatic bound plasma clearance. Stereoselectivity effect was reported by the ratio of the unbound clearance and the predicted in vivo clearance for each pair of stereoisomers.

[a] UGT $CL_{int}$ in presence of BSA was used for the calculation of the combined unbound clearance. Error margins for the clearances were calculated based on the rules of the Gaussian error propagation but without consideration of uncertainty in $f_{u,inc}$ and $f_{u,plasma}$. and the blood plasma partitioning.

[b] Data are reported considering a BLQ of 1 µL/min/mg in UGT and CYP metabolism conditions

DMD Fast Forward. Published on December 7, 2022 as DOI: 10.1124/dmd.122.001024
This article has not been copyedited and formatted. The final version may differ from this version.

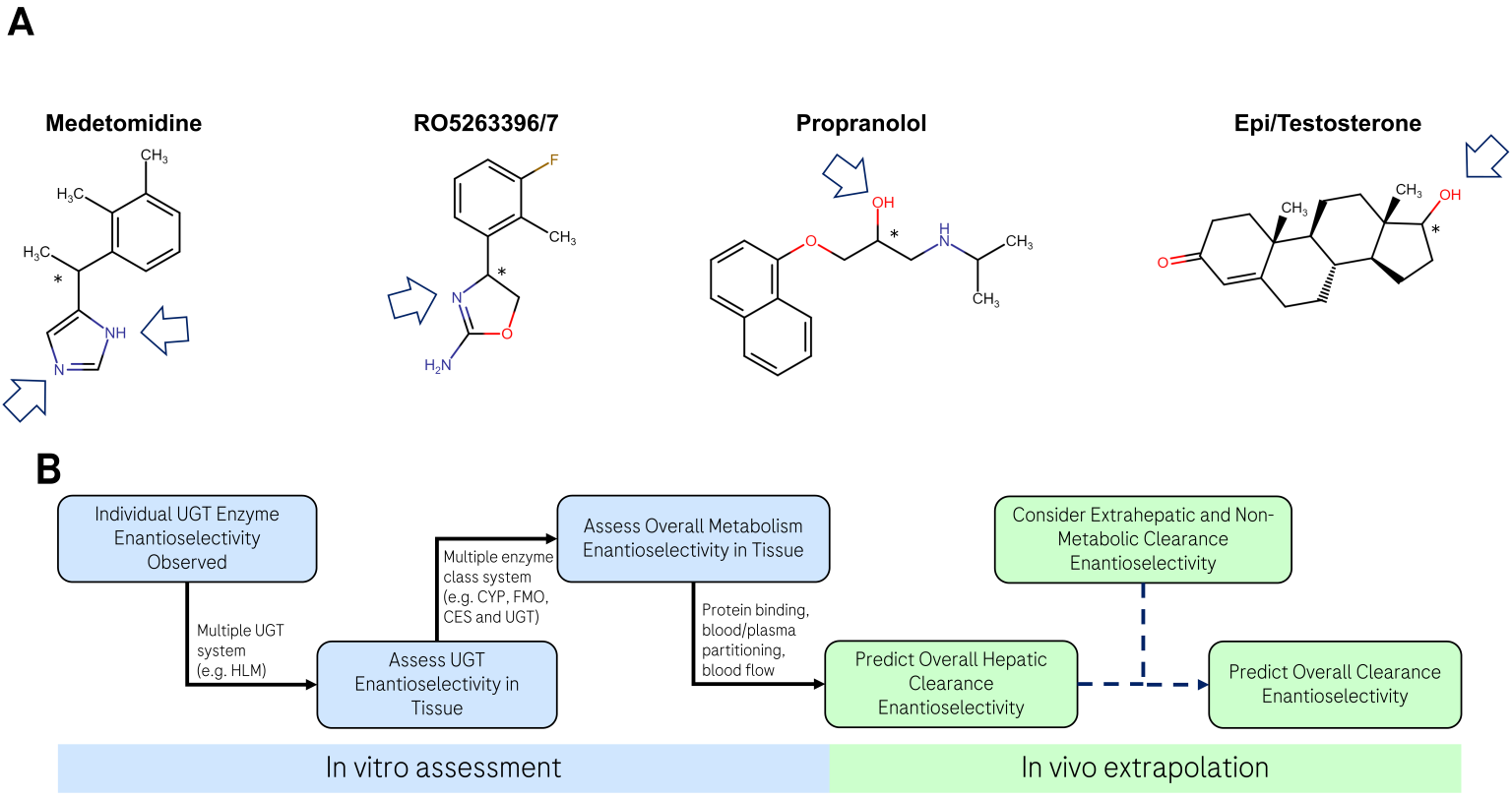


Fig.1

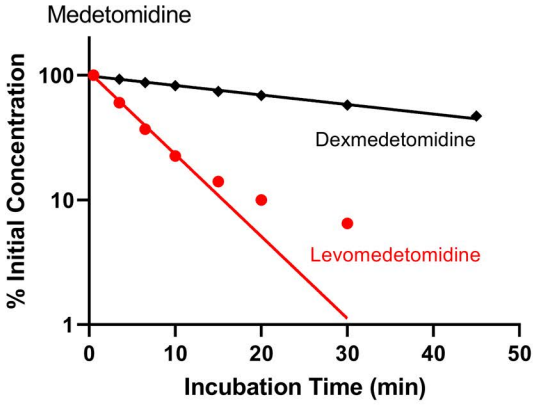
Medetomidine
% Initial Concentration
100
10
1
0
10
20
30
40
50
Incubation Time (min)
Dexmedetomidine
Levomedetomidine

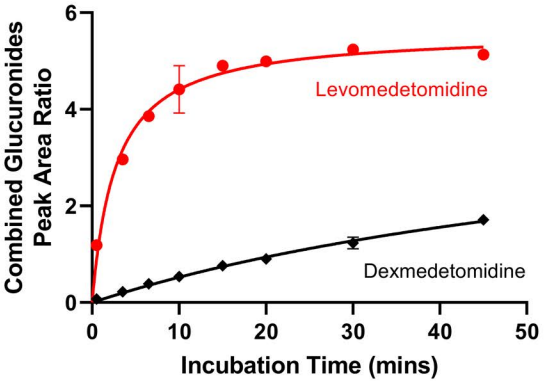
Combined Glucuronides
Peak Area Ratio
6
4
2
0
0
10
20
30
40
50
Incubation Time (mins)
Levomedetomidine
Dexmedetomidine

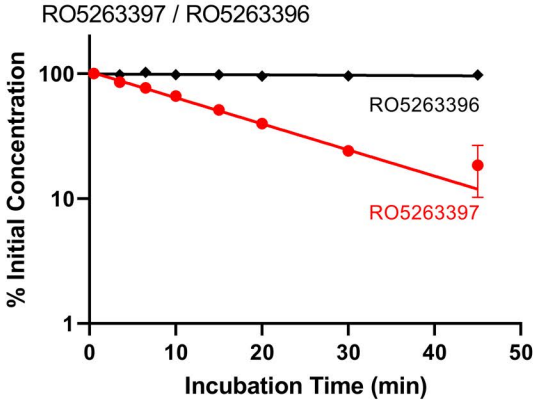
RO5263397 / RO5263396
% Initial Concentration
100
10
1
0
10
20
30
40
50
Incubation Time (min)
RO5263396
RO5263397

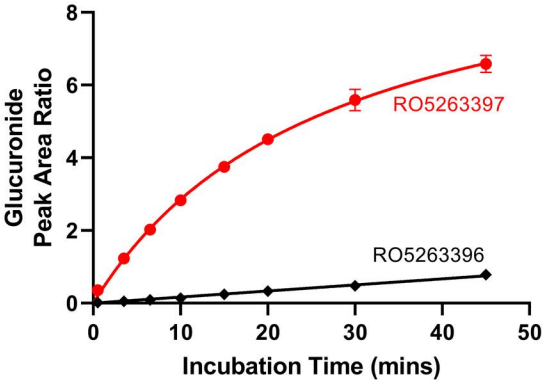
Glucuronide
Peak Area Ratio
8
6
4
2
0
0
10
20
30
40
50
Incubation Time (mins)
RO5263397
RO5263396

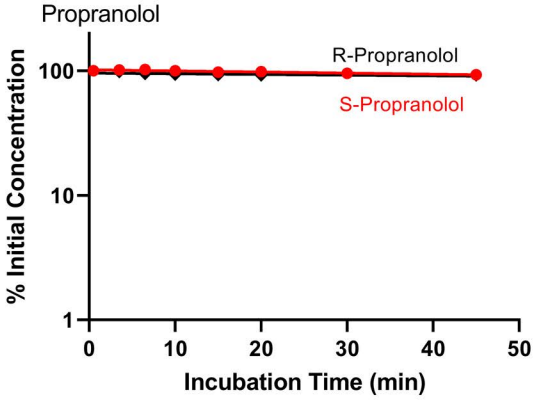
Propranolol
% Initial Concentration
100
10
1
0
10
20
30
40
50
Incubation Time (min)
R-Propranolol
S-Propranolol

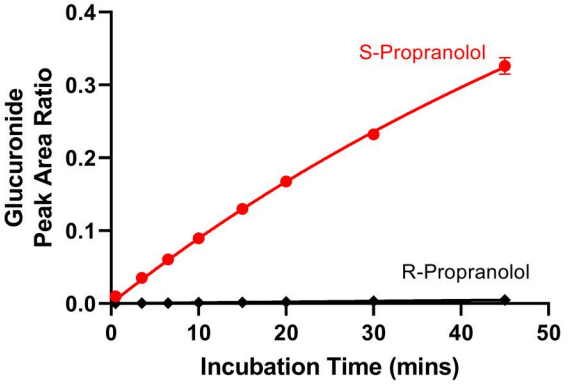
Glucuronide
Peak Area Ratio
0.4
0.3
0.2
0.1
0.0
0
10
20
30
40
50
Incubation Time (mins)
S-Propranolol
R-Propranolol

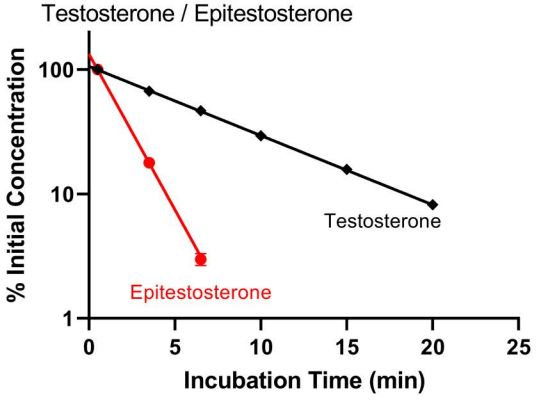
Testosterone / Epitestosterone
% Initial Concentration
100
10
1
0
5
10
15
20
25
Incubation Time (min)
Testosterone
Epitestosterone

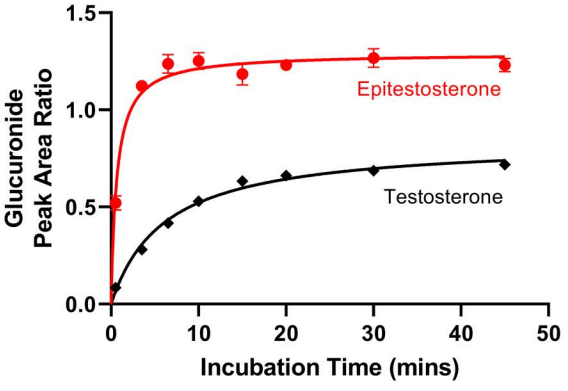
Glucuronide
Peak Area Ratio
1.5
1.0
0.5
0.0
0
10
20
30
40
50
Incubation Time (mins)
Epitestosterone
Testosterone

Fig.2

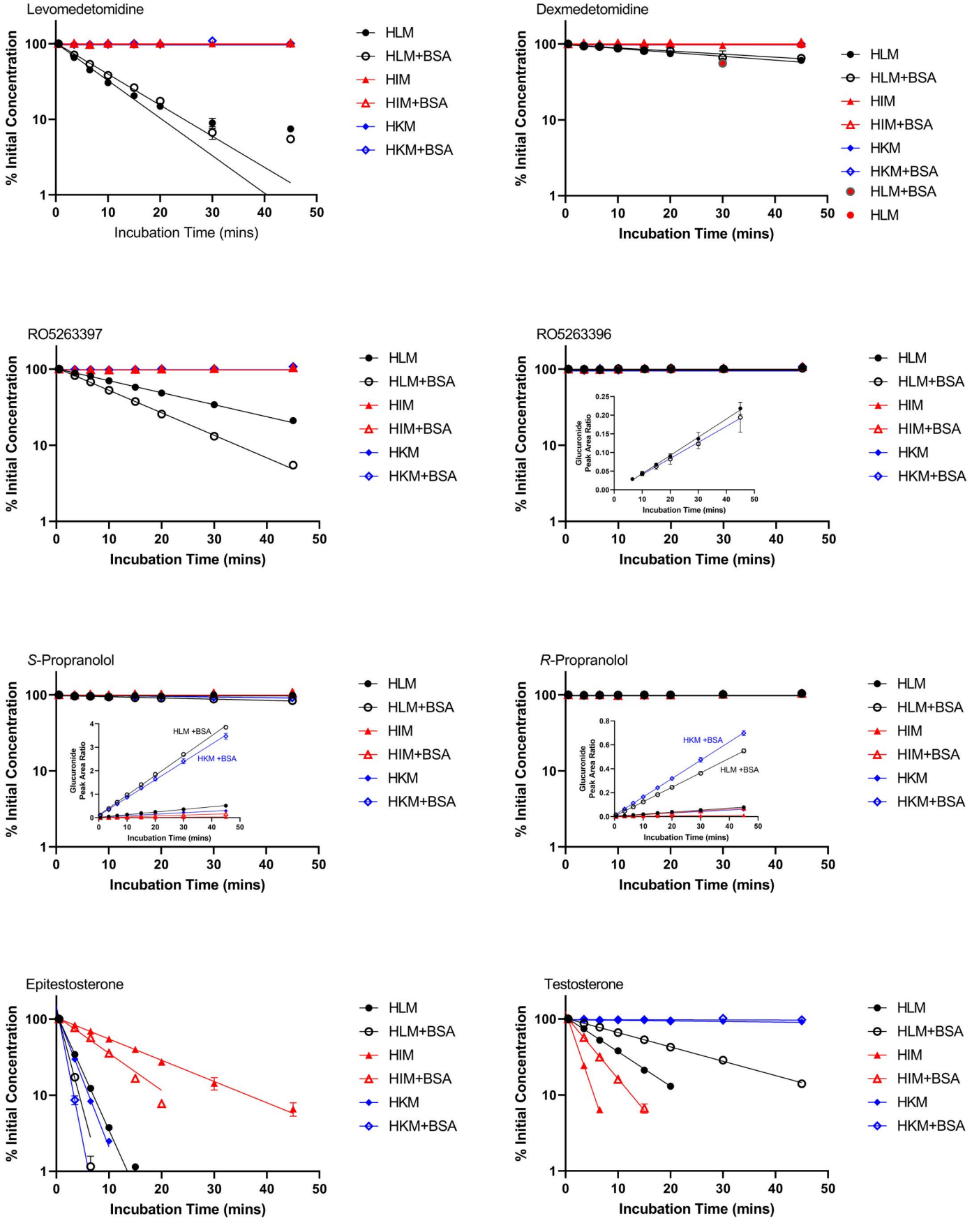
Levomedetomidine
% Initial Concentration
Incubation Time (mins)
HLM
HLM+BSA
HIM
HIM+BSA
HKM
HKM+BSA
Dexmedetomidine
% Initial Concentration
Incubation Time (mins)
HLM
HLM+BSA
HIM
HIM+BSA
HKM
HKM+BSA
HLM+BSA
HLM
RO5263397
% Initial Concentration
Incubation Time (mins)
HLM
HLM+BSA
HIM
HIM+BSA
HKM
HKM+BSA
RO5263396
% Initial Concentration
Glucuronide Peak Area Ratio
Incubation Time (mins)
Incubation Time (mins)
HLM
HLM+BSA
HIM
HIM+BSA
HKM
HKM+BSA
S-Propranolol
% Initial Concentration
HLM +BSA
HKM +BSA
Glucuronide Peak Area Ratio
Incubation Time (mins)
Incubation Time (mins)
HLM
HLM+BSA
HIM
HIM+BSA
HKM
HKM+BSA
R-Propranolol
% Initial Concentration
HKM +BSA
HLM +BSA
Glucuronide Peak Area Ratio
Incubation Time (mins)
Incubation Time (mins)
HLM
HLM+BSA
HIM
HIM+BSA
HKM
HKM+BSA
Epitestosterone
% Initial Concentration
Incubation Time (mins)
HLM
HLM+BSA
HIM
HIM+BSA
HKM
HKM+BSA
Testosterone
% Initial Concentration
Incubation Time (mins)
HLM
HLM+BSA
HIM
HIM+BSA
HKM
HKM+BSA

Fig.3

DMD Fast Forward. Published on December 7, 2022 as DOI: 10.1124/dmd.122.001024


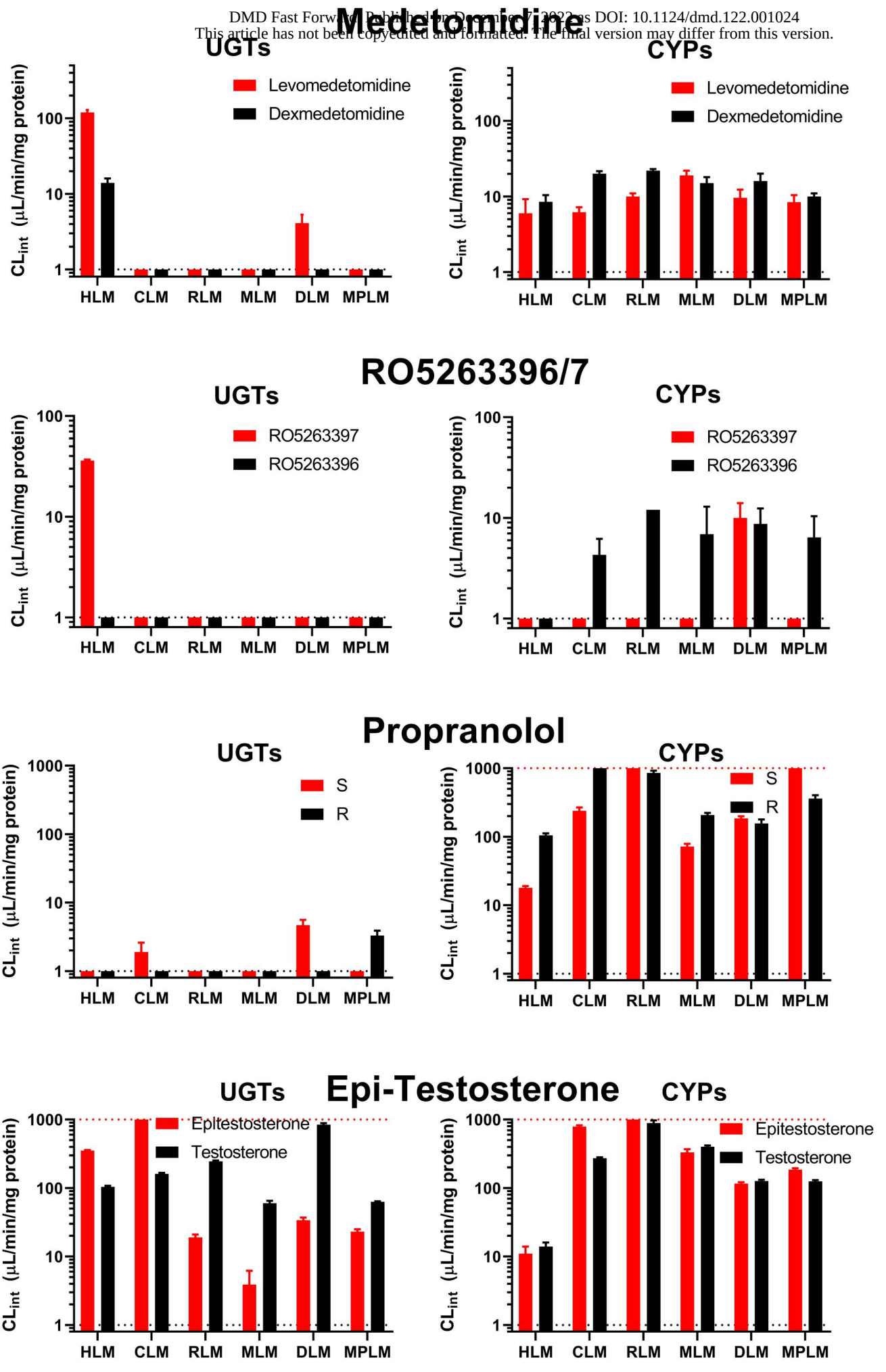


Fig.4

DMD Fast Forward. Published on December 7, 2022 as DOI: 10.1124/dmd.122.001024
This article has not been copyedited and formatted. The final version may differ from this version.

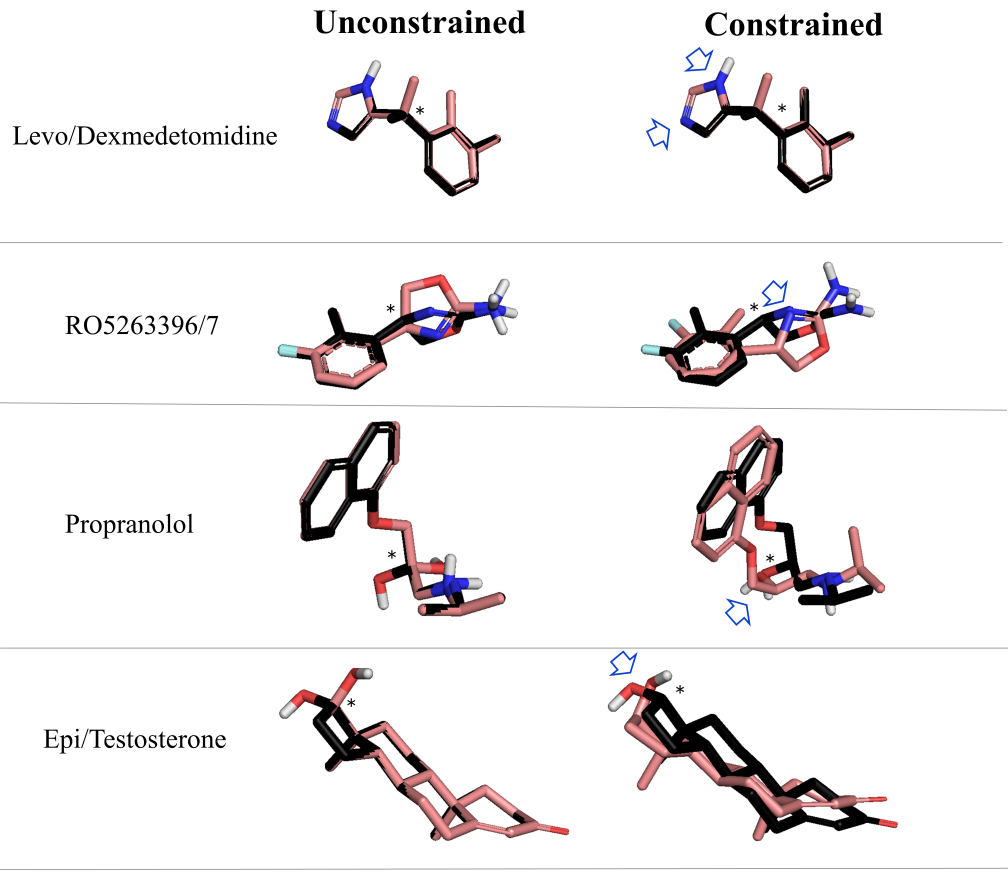


Fig.5

**Drug Metabolism and Disposition article DMD-AR-2022-001024**

# Contribution of UGT enzymes to human drug metabolism stereoselectivity: a case study of medetomidine, RO5263397, propranolol and testosterone

## Supplemental Information

Nicolò Milani, NaHong Qiu and Stephen Fowler

Pharmaceutical Sciences, Roche Pharma Research and Early Development, Roche Innovation Centre Basel, Grenzacherstrasse 124, 4070, Basel, Switzerland (NM, NQ, SF) and Department of Chemistry, Biology and Biotechnology, University of Perugia, 06123 Perugia, Italy (NM).

**Turnover of RO5263397 and RO5263396 by recombinantly expressed UGT2B10 and UGT1A4**

*Experimental Method:*

UGT2B10 and UGT1A4 were prepared in the same Tris buffer as HLM, but at a protein concentration of 0.55 mg/mL (final concentration: 0.50 mg/mL) and without the pre-treatment with alamethicin. Incubation procedure was as for UGT incubations described above; RO5263397, RO5263396 and medetomidine enantiomers were incubated at a concentration of 1µM. Sampling points were: 0.5, 3.5, 6.5, 10, 15, 30, 45, and 90 minutes and 40 µL of each incubation mixture was removed and pipetted into 384-well deep well plates preloaded with 80 µL quench solution (chilled acetonitrile containing 500 ng/mL of $D_6$-midazolam as internal standard).

*Results:*

RO5263397 has previously been shown to be selectively metabolized by UGTs and in particular by UGT2B10 (Fowler et al., 2015; Milani et al., 2020); intrinsic clearance of its enantiomer RO5263396 by UGTs was not measurable and the glucuronide formation rate was not quantifiable and it demonstrated a very high UGT metabolic stability of RO5263396 (Supplementary Information Figure S1). Levomedetomidine and dexmedetomidine were metabolized by UGT2B10 with intrinsic clearances of 27 ± 1 and 2.6 ± 0.3 µL/min/mg, respectively. (UGT1A4 Clint values were below limit of quantitation.) Therefore the most active isomer UGT2B10 metabolized levomedetomidine 10-fold faster than dexmedetomidine. Conversely, the metabolism of dexmedetomidine was indicated by the metabolite peak formation rates to be 2-fold faster than that of levomedetomidine in recombinant UGT1A4 incubations.

**Figure S1. Activity of UGT2B10 and UGT1A4 enzyme preparations in the metabolism of RO5263397/6 and Medetomidine**

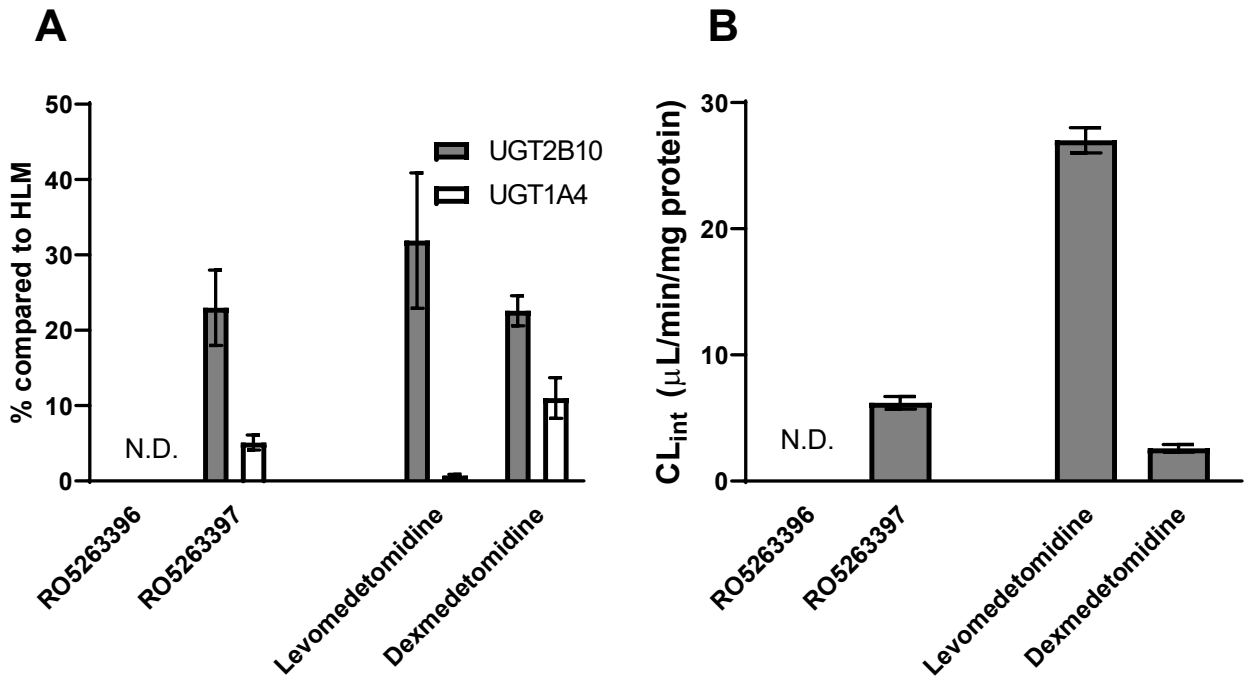


A) Activity of UGT2B10 and UGT1A4 for RO5263396/7 and medetomidine enantiopairs as percentage of clearance in the HLM.

B) $CL_{int}$ in the recombinant UGT2B10 incubations.

N.D. not detectable since it was below the limit of quantification (1 µL/min/mg)

**Supplemental Table 1: Measured Intrinsic Clearances of Medetomidine, RO5263397, Propranolol and Testosterone in Liver Microsomes without BSA Supplementation**

| Compound | | Medetomidine | | | RO5263397/6 | | | Propranolol | | | Testosterone | | |
|---|---|---|---|---|---|---|---|---|---|---|---|---|---|
| | | Levo | Dex | Ratio | RO5263397 | RO5263396 | Ratio | S | R | Ratio | Epi | Test | Ratio |
| | | µL/min/mg | | | µL/min/mg | | | µL/min/mg | | | µL/min/mg | | |
| Human | UDPGA* | 120 ±9 | 14 ±2 | 8.6 | 36 ±1 | BLQ | > 36 | BLQ | BLQ | ND | 353 ±5 | 105 ±4 | 3.4 |
| | NADPH | 6.0 ±3.2 | 8.5 ±1.9 | 0.49 | BLQ | BLQ | ND | 18 ± 1 | 105 ±7 | 0.17 | 11 ±3 | 14 ±2 | 0.79 |
| | Sum | 1 | 22.5 | 5.6 | 36 | BLQ | 36 | 18 | 105 | 0.17 | 364 | 119 | 3.1 |
| Cynomolgus | UDPGA | BLQ | BLQ | ND | BLQ | BLQ | ND | 1.9 ± 0.7 | 1.2 ± 0.5 | 1.6 | >1000 | 161 ±6 | >6.2 |
| | NADPH | 6.2 ±1 | 20 ±1.6 | 0.31 | BLQ | 4.3 ±1.9 | <0.23 | 240 ±28 | >1000 | <0.24 | 793 ±30 | 273 ±8 | 2.9 |
| Rat | UDPGA | BLQ | BLQ | ND | BLQ | BLQ | ND | BLQ | BLQ | ND | 19 ±2 | 245 ±8 | 0.076 |
| | NADPH | 10 ±1 | 22 ±1 | 0.45 | BLQ | 12 ±5 | <0.083 | >1000 | 852 ±71 | >1.2 | >1000 | 890 ±86 | >1.1 |
| Mouse | UDPGA | BLQ | BLQ | ND | BLQ | BLQ | ND | BLQ | BLQ | ND | 3.9 ± 2.3 | 60 ±5 | 0.065 |
| | NADPH | 19 ±3 | 15 ±3 | 1.3 | BLQ | 6.9 ±6.0 | <0.14 | 72 ±7 | 208 ±15 | 0.35 | 333 ±36 | 402 ±17 | 0.812 |
| Dog | UDPGA | 4.1 ±1.2 | BLQ | >4.1 | BLQ | BLQ | ND | 4.7 ±0.9 | BLQ | >4.7 | 34 ±3 | 843 ±42 | 0.040 |
| | NADPH | 9.6 ±2.7 | 16 ±4 | 0.60 | 10 ± 4 | 8.7 ±3.7 | 1.1 | 186 ±13 | 156 ±23 | 1.2 | 116 ±6 | 127 ±5 | 0.91 |
| Minipig | UDPGA | BLQ | BLQ | ND | BLQ | BLQ | ND | BLQ | 3.3 ±0.6 | <0.30 | 23 ±2 | 63 ±1 | 0.40 |
| | NADPH | 8.4 ±2.0 | 10 ±1 | 0.84 | BLQ | 6.4 ±4.0 | <0.16 | >1000 | 360 ±43 | >2.8 | 185 ±9 | 125 ±6 | 1.5 |

*Relative rates of initial glucuronide formation by pooled HLM assuming equal LC-MS/MS response of glucuronides: RO5263397/RO5263396: 74; S-Propranolol/R-Propranolol: 6.6 (see also Supplemental Table 2)

notes: sum only calculated for man since the rest is descriptive; values not calculated where $CL_{int}$ < 1 µL/min/mg; values are a starting point

BLQ: not determined since the $CL_{int}$ was below the limit of quantification (1 µL/min/mg)

ND: not determined

**Supplemental Table 2: Measured (Bound) intrinsic Clearance and Calculated Unbound Intrinsic Clearances of Medetomidine, RO5263397, Propranolol and Testosterone in Incubations with Pooled HLM in presence and absence of BSA.**

| | **$CL_{int}$** | | | | | | **Glucuronide Peak Appearance Rate (Peak Area Glucuronide/Peak Area Internal Standard per minute)** | | | | | |
|---|---|---|---|---|---|---|---|---|---|---|---|---|
| | **Medetomidine** µL/min/mg | | | **Epi/Testosterone** µL/min/mg | | | **RO5263396/7** | | | **Propranolol** | | |
| | Levo | Dex | Ratio[a] | Epi | Test | Ratio[a] | S | R | Ratio[a] | S | R | Ratio[a] |
| - BSA observed | 120 | 14 | 8.6 | 353 | 104 | 3.4 | 0.35 | 0.0047 | 74 | 0.011 | 0.0017 | 6.6 |
| + BSA observed | 96 | 11 | 8.7 | 597 | 43 | 14 | 0.56 | 0.0043 | 130 | 0.085 | 0.012 | 7.0 |
| | | | | | | | | | | | | |
| - BSA free fraction corrected | 235 | 26 | 9.0 | 559 | 149 | 3.8 | 0.51 | 0.0067 | 77 | 0.085 | 0.0044 | 6.6 |
| + BSA free fraction corrected | 300 | 34 | 8. 7 | 5012 | 424 | 12 | 0.82 | 0.0059 | 139 | 0.40 | 0.029 | 14 |
| | | | | | | | | | | | | |
| ratio $CL_{int}$+BSA/-BSA[b] | 0.80 | 0.79 | | 1.7 | 0.41 | | 1.6 | 0.91 | | 7.6 | 7.1 | |
| ratio unbound $CL_{int}$+BSA/-BSA[c] | 1.3 | 1.3 | | 9.0 | 2.5 | | 1.6 | 0.89 | | 14 | 6.6 | |

[a] Ratio between $CL_{int}$ or $CL_{int,u}$ for the respective enantiomers

[b] Effect of BSA for each enantiomer on the $CL_{int}$

[c] Effect of BSA for each enantiomer on the $CL_{int,u}$

**Supplemental Table 3: Glucuronide formation ratio of S and R propranolol in presence and absence of BSA in HLM , HIM, and HKM.**

| | | Glucuronide formation rate | | | | | |
|---|---|---|---|---|---|---|---|
| Enantiomer | Condition | HLM | Ratio | HIM | Ratio | HKM | Ratio |
| S-propranolol | No BSA | 0.0112 ± 0.003 | 7.6 | $7.4\ 10^{-4} \pm 1\ 10^{-5}$ | 5.0 | 0.0062± 0.0003 | 12 |
| | BSA | 0.085 ± 0.001 | | 0.0037± 0.0001 | | 0.076± 0.002 | |
| R-propranolol | No BSA | 0.00170 ± 0.00051 | 7.1 | $2.4\ 10^{-4} \pm 1\ 10^{-5}$ | 6.5 | 0.00124± 0.00007 | 12 |
| | BSA | 0.0121 ± 0.0002 | | 0.00157± 0.00003 | | 0.0153±0.0003 | |

## Supplemental Table 4: MS/MS parameters and retention time for all enantiomers

| Parent | | | | Metabolite | | | DP (Volts) | CE (Volts) |
|---|---|---|---|---|---|---|---|---|
| **Compound** | **Chromatography*** | **Q1-Q3** | **RT** (min) | **Q1-Q3** | **Conf.** | **RT** (min) | | |
| Medetomidine | A | 201.0-94.9 | 0.65 | 377.0-201.0 | Levo | 0.70 | 70 | 25 |
| | | | | | Dex | 0.68 | | |
| RO5263396/ RO5263397 | B | 195.1-152.1 | 0.58 | 371.1-195.1 | R | 0.55 | 76 | 21 |
| | | | | | S | 0.62 | | |
| Propranolol | C | 260.2-116.1 | 0.66 | 436.2-260.2 | R | 0.67 | 70 | 25 |
| | | | | | S | 0.77 | | |
| Epi/Testosterone | B | 289.2-109 | 1.38 | 465.289.2 | Epi. | 1.18 | 80 | 30 |
| | | | 1.31 | | Test. | 1.11 | | |

*See Table 5

**Supplemental Table 5: Chromatography programs of all enantiopairs**

| Medetomidine (A) | | |
|---|---|---|
| Column | ACQUITY UPLC BEH C18 Column, 130Å, 1.7 µm, 2.1 mm X 50 mm | |
| Column Temp. (°C) | 50 | |
| Injection volume | 2 µL | |
| Solvent A | Water + 0.1% HCOOH | |
| Solvent B | AcN + 0.1% HCOOH | |
| Time (min) | **% Solvent B** | **Flow (mL/min)** |
| 0 | 15 | 0.6 |
| 1.30 | 40 | |
| 1.31 | 98 | 1.2 |
| 1.60 | 98 | |
| 1.61 | 15 | |
| 2.00 | 15 | 0.6 |

| RO5263396/7 & Epi_Testosterone (B) | | |
|---|---|---|
| Column | ACQUITY UPLC BEH C18 Column, 130Å, 1.7 µm, 2.1 mm X 50 mm | |
| Column Temp. (°C) | 50 | |
| Injection volume | 2 µL | |
| Solvent A | Water + 0.1% HCOOH | |
| Solvent B | AcN + 0.1% HCOOH | |
| Time (min) | **% Solvent B** | **Flow (mL/min)** |
| 0 | 5 | 0.6 |
| 1.29 | 60 | |
| 1.30 | 98 | 1.2 |
| 1.60 | 98 | |
| 1.61 | 5 | |
| 2.00 | 5 | 0.6 |

| Propranolol (C) | | |
|---|---|---|
| Column | ACQUITY UPLC BEH C18 Column, 130Å, 1.7 µm, 2.1 mm X 50 mm | |
| Column Temp. (°C) | 50 | |
| Injection volume | 2 µL | |
| Solvent A | Water + 0.1% HCOOH | |
| Solvent B | AcN + 0.1% HCOOH | |
| Time (min) | **% Solvent B** | **Flow (mL/min)** |
| 0 | 15 | 0.6 |
| 1.30 | 45 | |
| 1.31 | 98 | 1.2 |
| 1.60 | 98 | |
| 1.61 | 15 | |
| 2.00 | 15 | 0.6 |